C.D.I. Report No. 87-02

FEASIBILITY OF AN ONBOARD WAKE VORTEX AVOIDANCE SYSTEM

Prepared by

Alan J. Bilanin
Milton E. Teske
Howard C. Curtiss, Jr.

CONTINUUM DYNAMICS, INC.
P.O. BOX 3073
PRINCETON, NEW JERSEY 08543

Prepared under Contract No. NAS1-17742 for

NATIONAL AERONAUTICS AND SPACE ADMINISTRATION
LANGLEY RESEARCH CENTER
HAMPTON, VIRGINIA 23665

and

under Contract No. DTRS-57-85-C- 000123 for

DEPARTMENT OF TRANSPORTATION
TRANSPORTATION SYSTEMS CENTER
KENDALL SQUARE
CAMBRIDGE, MASSACHUSETTS 02142

April 1987

TABLE OF CONTENTS

1. INTRODUCTION

1.1 Identification and Significance of the Problem or Opportunity

The FAA is currently expending a great deal of effort in determining means that could lead to capacity and efficiency gains in the National Airspace System (NAS). Planned NAS modernization improvements will accommodate the projected traffic growth, but safety considerations may limit utilization of the economies anticipated by these improvements. Currently, the wake vortex hazard is a major safety consideration which may limit the NAS to accommodate future growth.

IFR separation standards are currently 3/4/5/6 nmi (depending on the generator/encounter aircraft combination). The FAA estimates significant traffic increases at most airports over the next twenty years, and IFR delays will get worse. The MITRE Corporation, in studies for the FAA (Ref. 1), has shown that if the vortex wake hazard could be eliminated, the NAS could accommodate separations of 2.5 nmi and greatly reduce this hazard. NASA has pursued aerodynamic alleviation at the source to reduce the intensity of the vortices, while the FAA has pursued a ground based detection and avoidance system.

The NASA program (Refs. 2-4) has demonstrated that aerodynamic alleviation is possible, but to date these concepts are only partially successful. The concepts, when deployed on existing aircraft, all have performance and/or efficiency penalties. In addition, the concepts have been shown to be sensitive to small aerodynamic changes (such as extending landing gear, Refs. 5 and 6). Since no general alleviation concept has been developed, NASA has revised its program to emphasize vortex physics with the hope of developing alleviation concepts which can be factored into the design of the next generation of jetliners. In any event, vortex alleviation at the source seems to be a long way off.

The second concept to reduce vortex hazard, under development by the FAA, is to monitor the position of vortices using ground based sensors. A recent workshop, held in September of 1983 at NASA Langley, addressed Wake Vortex Detection Technology and identified several promising sensor technologies.

These technologies were either land based or airborne. The workshop concluded, however, that operational readiness of any system is at least ten years away.

The need for an interim system which will allow pilots to close separations during IFR conditions is immediate. Under VFR conditions, pilots voluntarily reduce spacings to 2 nmi or less. If an onboard vortex detection system could be developed which would be reliable and inexpensive, and give pilots a level of confidence against vortex encounter by giving a warning of an imminent encounter, as well as evasive action, aircraft separations under IFR conditions may be reduced. This report investigates the feasibility of developing an interim onboard vortex avoidance system. This system would use existing proven sensors such as angle-of-attack vanes, roll rate sensors and/or accelerometers and might become part of an existing avoidance system such as a wind-shear detection system.

1.2 Phase I Study Objectives

The Phase I study reported herein attempts to answer the following questions.

1) Using existing instrumentation how far from vortex cores can a vortex signature be detected?

2) Can this signature be used to compute location of a vortex wake?

3) How large is the signal to noise?

4) Will this signal be adequate to provide detection and evasion time for in trail encounters?

5) Are there any other reasons why the proposed concept might not work?

Complete answers to these questions, because of the limited scope of the Phase I effort, cannot be given, but sufficient progress has been made to determine if a Phase II research effort is justified. The remainder of this report addresses the above five questions.

2. DETECTABILITY

2.1 Idealized Signal Strength

The wake of an aircraft is made up of two-counter rotating vortices known as a vortex pair. In Figure 1 is shown a schematic of an encountering aircraft about to interact with the wake of a generator aircraft during approach. Note that the wake of the generator extends aft of the encountering aircraft, but in this schematic it is truncated at a transverse plane located at the wing of the encountering plane. This plane will be used often to discuss vortex detection in the remainder of this report. Note that the wake shown schematically in this figure is not straight along the generator aircraft's landing trajectory but is shown distorted. This distortion results from a wake instability which must be accounted for in a wake detector algorithm. This instability, known as sinusoidal instability, is one source of noise which will complicate the detection algorithm. Noise will be a significant but surmountable problem in developing an onboard vortex detector system.

In the transverse or analysis plane, Figure 2 shows schematically the location of the vortex centers and location of an encountering aircraft relative to the vortex pair. The strength of the vortex is quantified by the circulation, Γ , and the spacing between the vortices, b , is nominally about 2/3 the wingspan of the generating aircraft. It is well known that the weight of the generating aircraft is related to the air density, ρ , and flight speed, U , by Weight = $\rho U \Gamma b$. The product of Γb is known as the dipole coefficient, $\mu = \Gamma b$, and to a good approximation determines the magnitude of the swirling velocity field for radial distances $R > b$ in the region where the encountering aircraft would first detect the presence of the vortex pair.

It is well known also that the velocity field in this analysis plane is to a good approximation given by

$$V = -\frac{\mu}{\pi}\frac{YZ}{R^4} \quad , \quad W = \frac{\mu}{2\pi}\frac{Y^2 - Z^2}{R^4} \qquad (1)$$

for $R > b$.

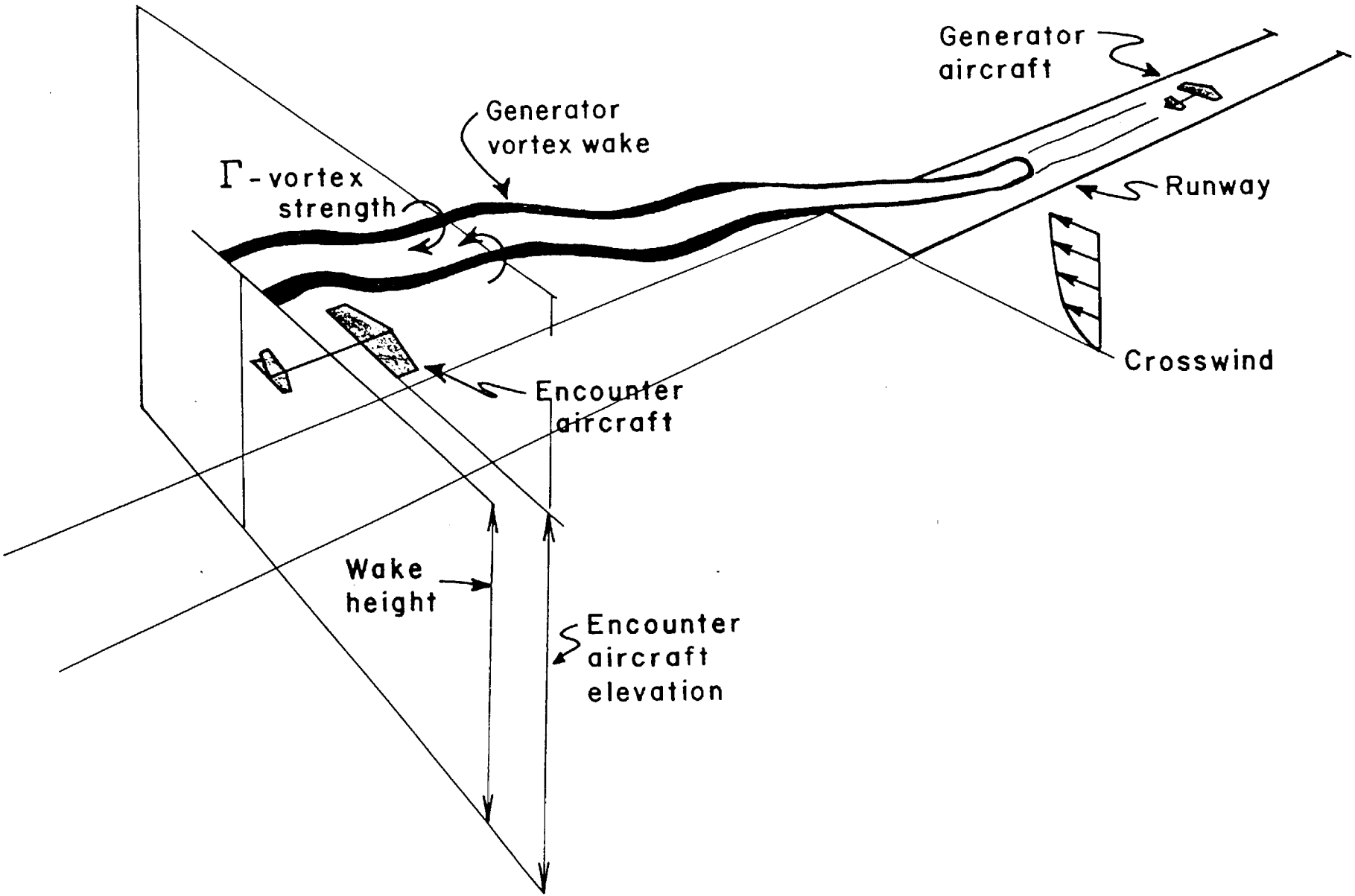

Figure 1. Schematic of a vortex wake encounter upon approach. Note that a crosswind advects the vortex pair and atmospheric turbulence results in a sinusoidal instability of the vortex system.

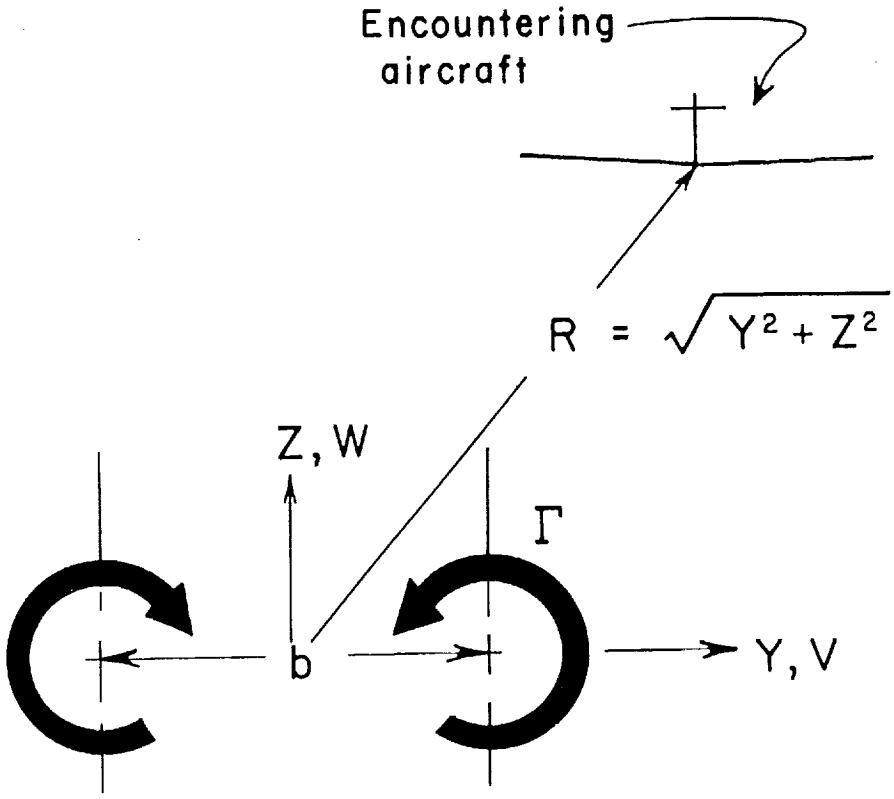

Figure 2. Schematic of an encountering aircraft in the vortex flow field of a generator. The cartesian cordinate system, Y , Z , has corresponding velocity components, V , W .

Hence, a key observation is made that the swirling velocities that characterize a wake flow field, V and W , are to first approximation proportional to the dipole coefficient, μ . Since all aircraft land at about the same speed (so as to maintain proper separation during approach) the dipole coefficient, μ , is related directly to the weight of the generating aircraft. This relationship between μ and Weight is tabulated on Table 1 and has been computed from data published in Aviation Week dated March 18, 1985. Note that in the units used the dipole coefficient is about twice the weight of the aircraft. Therefore, during landing approach the intensity of the vortex swirling velocity field is simply proportional to the weight of the generating aircraft. The structure of this velocity field which we may want to detect is shown in Figures 3 and 4. Here, lines of constant V and W are shown, respectively, for the wake of an aircraft weighing 550,000 lbs during landing approach. Note the complex structure of this velocity field, since it will be sensed by a detector system to determine vortex pair location.

It is worth noting that for this weight, aircraft vertical velocities are of the order of 1.0 ft/sec at distances 400 ft lateral offset from the centerline of the wake, and drop off as the square of the distance away from the dipole center. It is suggested that this velocity field, or the response which it induces on an encountering aircraft such as roll or rectilinear acceleration, be the signal from which a detection algorithm will determine the relative location of an encountering aircraft from the wake center.

2.2 Existing Sensor Technology

The sensors examined in this study are summarized in Table 2. They have been chosen based on:

a) prior or current use aboard aircraft,
b) high reliability, and
c) documented accuracy , sensitivity and threshold.

TABLE 1.

Published Landing Weights and Computed Dipole Coefficients for Major Transport Aircraft (Ref 7)

Aircraft	Weight (lb) (max landing)	μ (ft^3/sec)	μ/Weight ($ft^3/sec/lb$)
B707	228,000	458,000	2.0
B727	154,333	308,000	2.0
B737	106,750	213,000	2.0
B747	552,000	969,000	1.8
B757	198,000	398,000	2.0
B767	282,667	523,000	1.9
L-1011	365,500	637,000	1.7
DC-8	229,333	417,000	1.8
DC-9	101,020	208,000	2.1
MD	131,375	269,000	2.1
DC-10	383,250	715,000	1.9

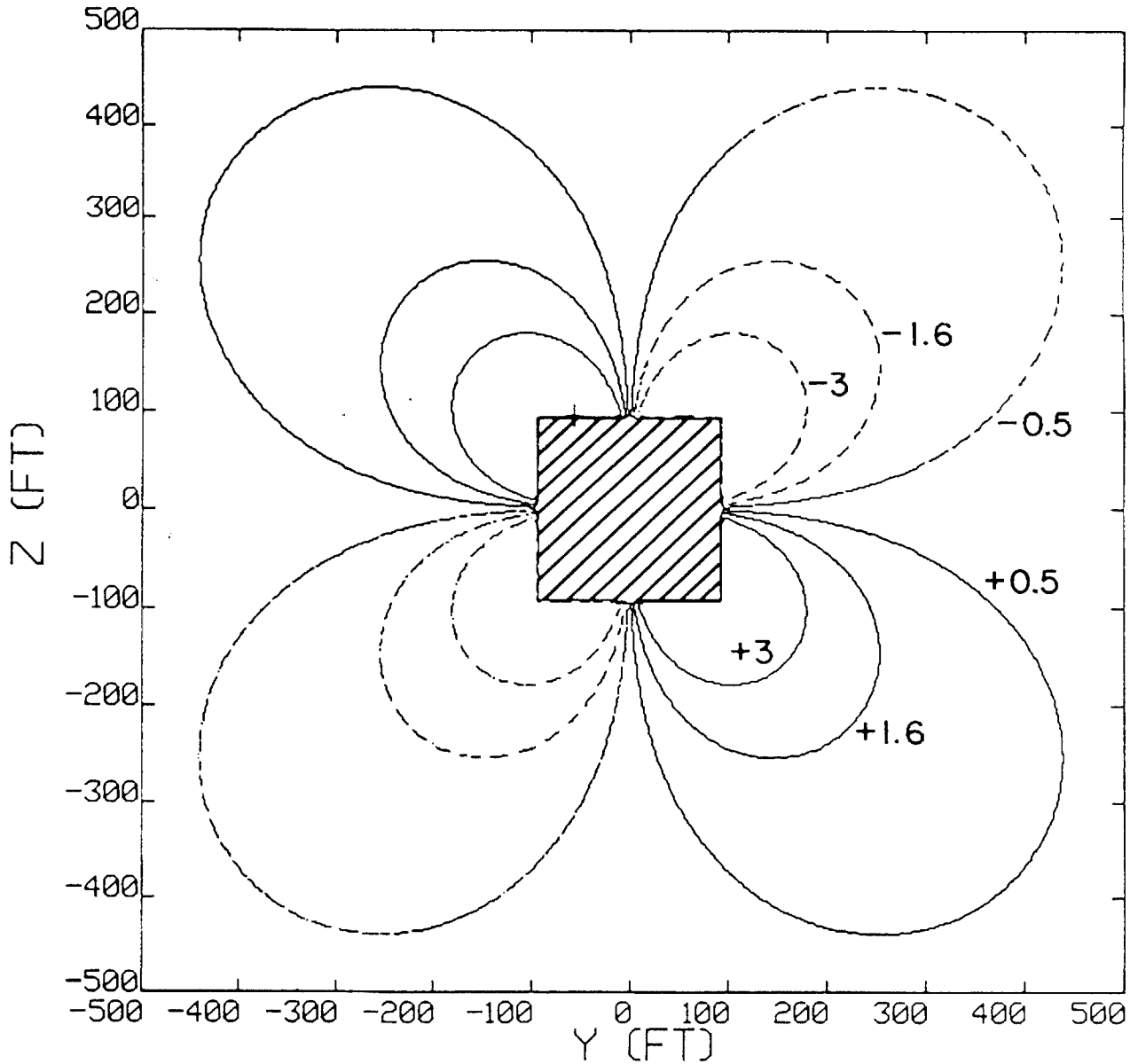

Figure 3. The horizontal velocity distribution, V , in the wake of a 550,000 lb aircraft during landing. Note that velocity isopleths are omitted in in the domain $|Y| < 100$ ft , $|Z| < 100$ ft where the dipole approximation is invalid. (Units of velocity contour ft/sec.)

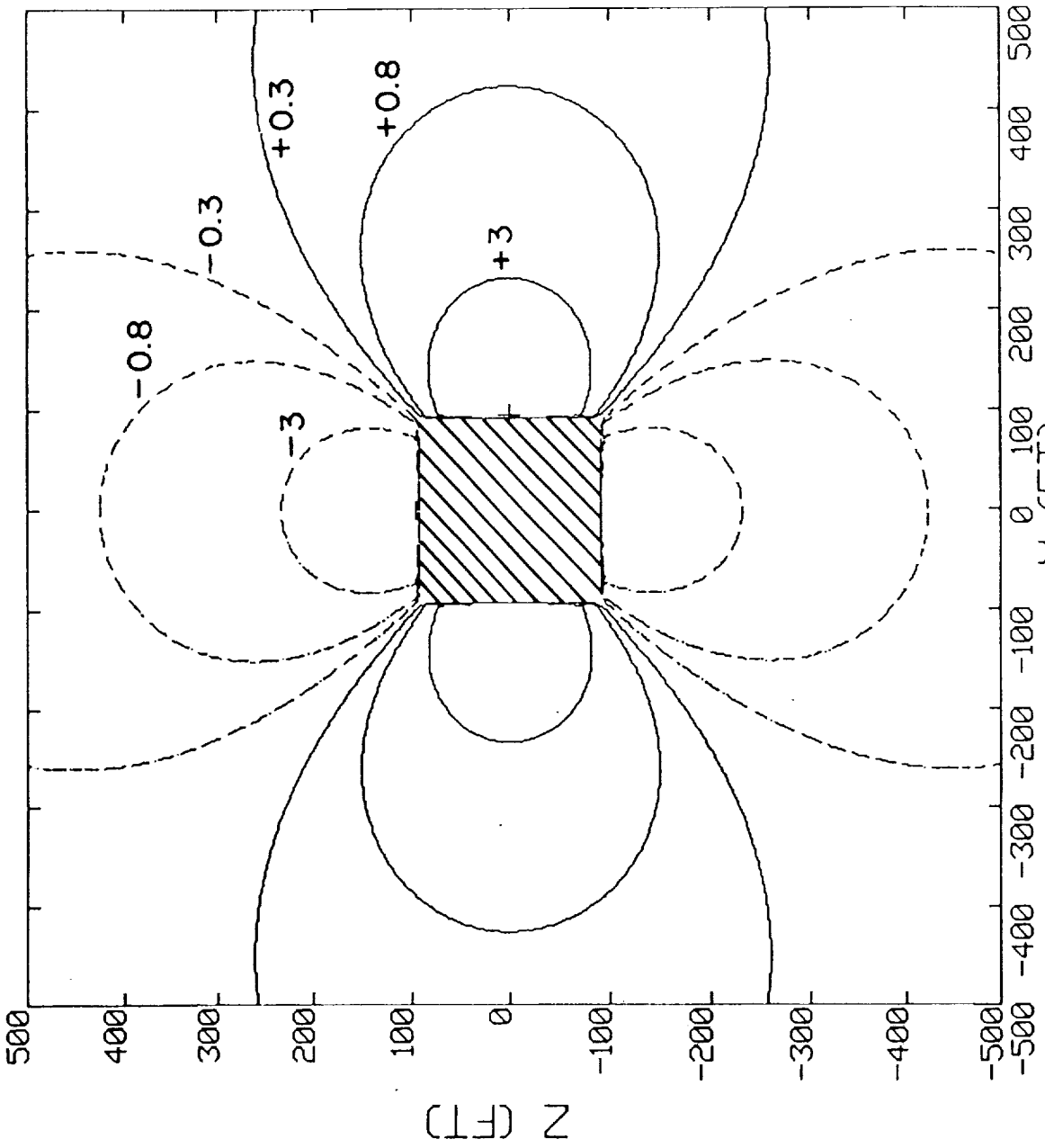

Figure 4. The vertical velocity distribution, W , in the wake of a 550,000 lb aircraft during landing. (Units of velocity contour ft/sec.)

TABLE 2a.

Tabulation of Instrument Sensors Considered for Detecting a Vortex Wake

AERODYNAMIC ANGLES

Variable	Instrument	Range	Accuracy	Threshold	Response	Manuf.	Aircraft
Angle of Attack	Vanes	±60°	±0.5***	±0.2° - 0.3°	*	Rosemount Inc. Aerospace Div.	727,737, 757,767
Side Slip**	Vanes	±60°	±0.5***	±0.2° - 0.3°	*	Rosemount Inc. Aerospace Div.	**

* Information yet to be obtained

** Most commercial aircraft use an on board computer to calculate the side slip angle from various instruments.

*** ±0.25° accuracy is possible on these instruments

TABLE 2b.

Tabulation of Instrument Sensors Considered for Detecting a Vortex Wake

ROLL RATE/ACCELERATION

Variable	Instrument	Range	Accuracy	Threshold	Response	Manuf.	Aircraft
Roll rate	Rate Gyro	60 deg/sec	±0.15 deg/sec	0.01 deg/sec	28 Hz	US Time Corporation	(Typical Characteristics)
	(Laser Inertial Navigation)	400 deg/sec	±0.1 deg/sec	±0.015 deg/sec	*	Honeywell Government & Aeronautical Products Div.	737-300,757,767
Roll Acceleration	Angular Accelerometer	5 rad/sec^2	±0.0003 rad/sec^2	2μ rad/sec	10 Hz	Systron Inertial Div.	**

* Information yet to be obtained

** Not installed on most commercial aircraft

TABLE 2c.

Tabulation of Instrument Sensors Considered for Detecting a Vortex Wake

VERTICAL VELOCITY/ACCELERATION

Variable	Instrument	Range	Accuracy	Threshold	Response	Manuf.	Aircraft
Vertical Velocity	Rate of Climb	6000 ft/min	±200 ft/min	*	*	United Instruments	737,757
Vertical Velocity	Laser Inertial Navigation	**	**	**	**	Honeywell	737,757
Vertical Acceleration	Linear Accelerometer	±130 ft/sec^2	±0.3 ft/sec^2 ***	0.03 ft/sec^2	*	Honeywell	737,757

* Information yet to be obtained

** This system integrates the velocity from the linear accelerometer. This accuracy depends on the air data computer.

*** ±0.03 ft/sec^2 is available.

The instruments are grouped into three categories based on what variables are sensed.

a) Fluid velocites in a plane perpendicular to the direction of motion of the encountering aircraft (Table 2a).

b) Rotary velocity or acceleration of the aircraft (Table 2b).

c) Rectilinear velocity or acceleration of the aircraft (Table 2c).

Certain sensors have been eliminated from consideration as a consequence of very slow response times. An example of such an instrument is a rate-of-climb indicator.

2.3 Ideal Detection Distances

We have shown above how the wake flow field is directly related to the weight of the generating aircraft and have tabulated instruments which may be used on an onboard vortex dectection system. Some simple estimates of ideal detection distances can now be made neglecting noise. The detection distances are denoted as ideal detection distances.

Detection Using Flow Angle Vanes

Using Eq. (1), the velocity in the analysis plane, Q, divided by the encountering aircraft's flight speed is

$$\frac{|Q|}{U} = \frac{\sqrt{w^2 + v^2}}{U} \equiv \frac{\mu}{2\pi R^2 U} \qquad (2)$$

which is the angle which would be measured on a flow angle vane mounted on an encountering aircraft. For the sake of discussion here and all subsequent discussions, it is assumed that the approach speed is 200 ft/sec. According

to Rosemount Inc.'s Aerospace Division, angle-of-attack vanes can routinely be manufactured to detect angle changes as small as 0.25° although 0.5° is commonly quoted. Using Eq. (2) distances at which commercial jet transport can be first detected are given on Table 3. Note that distances are computed assuming both 0.25° and 0.5° flow angle threshold instruments. Note that as expected the heavier the generator aircraft the greater the distance at which detection is first ideally possible. The tabulated results can be summarized by characterizing aircraft by landing weight. Detection distances are shown as a function of weight on Figure 5.

Detection Using an Onboard Roll Rate Sensor

The most predominant response of aircraft to an in trail encounter is roll. Investigators have even proposed that the hazard associated with a vortex encounter should be determined by comparing the roll upset to the roll control authority of the aircraft (Refs 8 and 9). A simple estimate of the ideal roll rate induced by the wake is to equate the roll rate, $\dot{\phi}$, to the horizontal gradient of the vertical velocity $\partial W/\partial Y$ or

$$\dot{\phi} = \frac{\partial W}{\partial Y} = \frac{\mu Y\,(-Y^2 + 3Z^2)}{\pi \qquad R^6} \tag{3}$$

The ideal induced roll rate is now a complicated function of position, unlike the induced angle. To make a detection estimate analogous to that in Figure 5, assume a lateral encounter ($Z = 0$) and note from instrument Table 2b that thresholds for roll rate sensors are 0.002 rad/sec. In Figure 6 is shown the lateral detection distance as a function of aircraft landing weight. This is to be compared with Figure 5 and it is noted that the distance at which detection is first possible, based on roll rate sensors, is comparable to using flow angle vanes.

TABLE 3.

Idealized detection distances, R_1 and R_2, assuming flow angle vanes which can detect angle changes of 0.5° and 0.25°, respectively

Generating Aircraft	Weight # (max landing)	μ (ft^3/sec)	R_1(ft)	R_2(ft)
B707	228,000	458,000	214	303
B727	154,333	308,000	175	248
B737	106,750	213,000	145	206
B747	552,000	969,000	310	440
B757	198,000	398,000	197	279
B767	282,667	523,000	228	323
L-1011	365,500	637,000	252	357
DC-8	229,333	417,000	204	289
DC-9	101,020	208,000	144	204
MD	131,375	269,000	164	232
DC-10	383,250	715,000	267	378

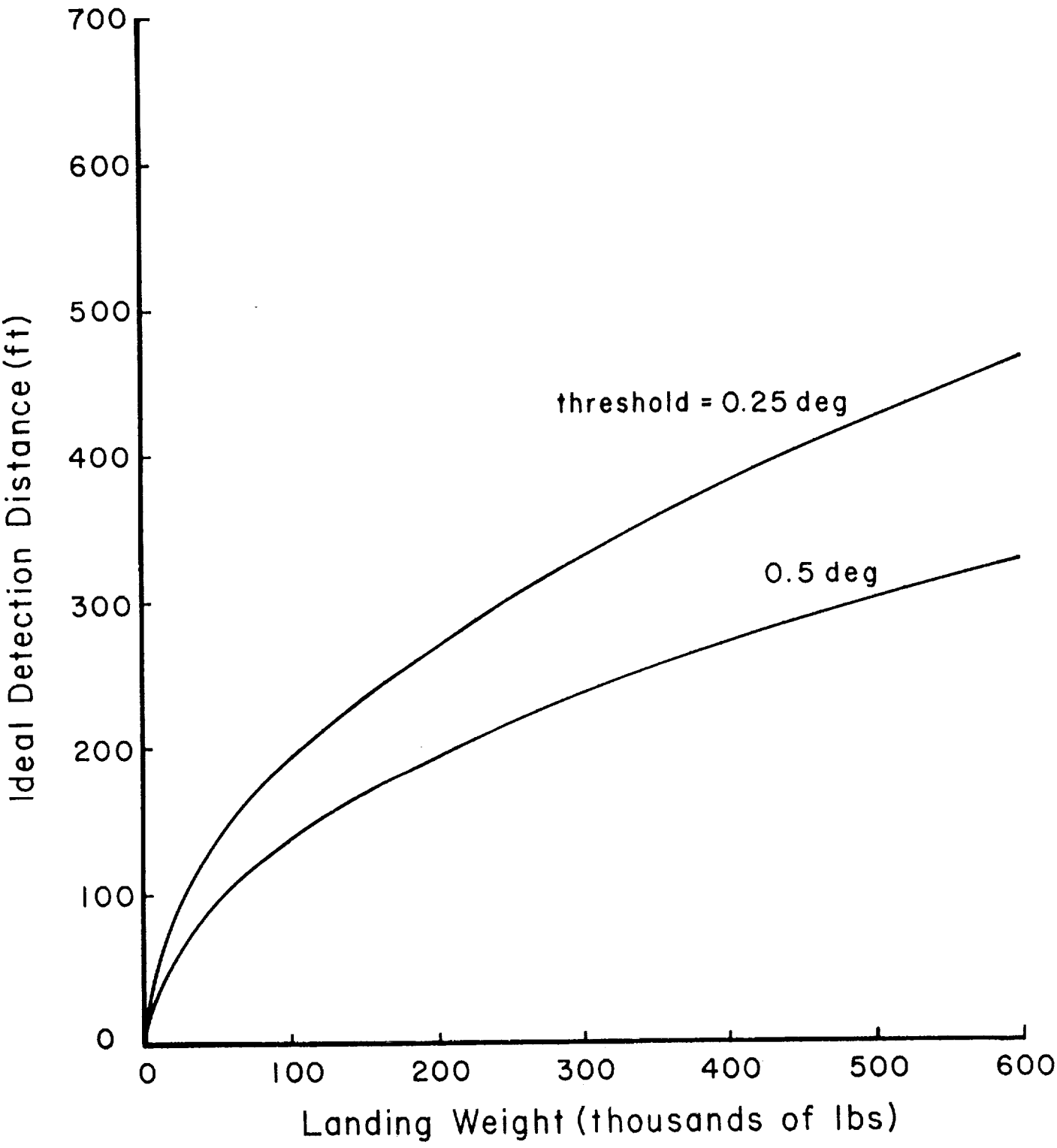

Figure 5. Detection distance using flow angle vanes as a function of aircraft landing weight and istrument threshold.

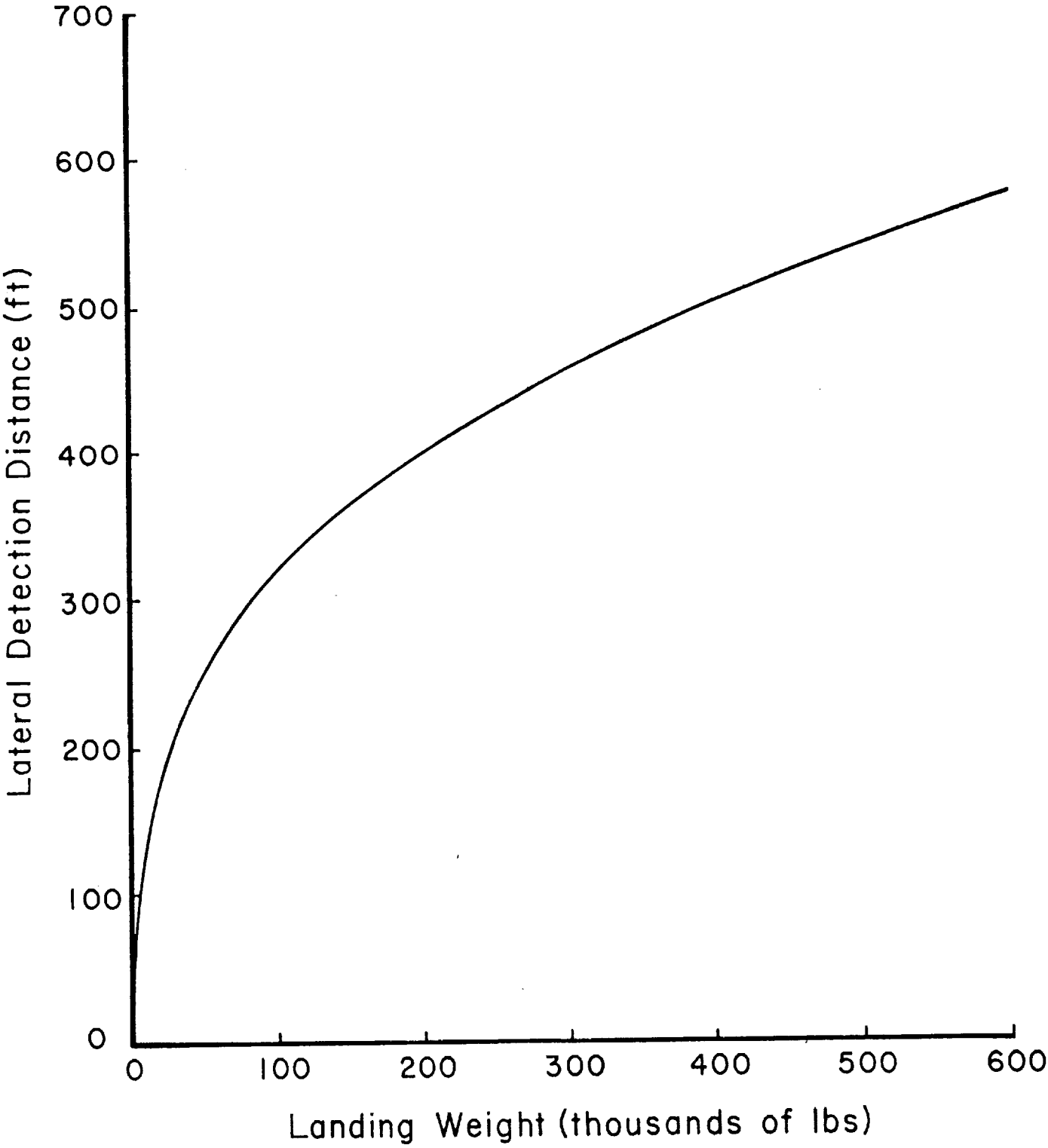

Figure 6. Lateral detection distance using roll rate sensor as a function of aircraft landing weight.

Detection Using an Onboard Rectilinear Accelerometer

Rectilinear accelerations are produced onboard as a consequence of changes in aerodynamics forces induced by the dipole flow field. Simple estimates of accelerations to be anticipated must be made using an aircraft dynamic model. A three-degree-of-freedom uncoupled model has been developed and coded to make these estimates. Roll (ϕ), pitch (θ) and lateral ($\ddot{y}$) and vertical ($\ddot{z}$) accelerations are computed using the conventions shown sketched below

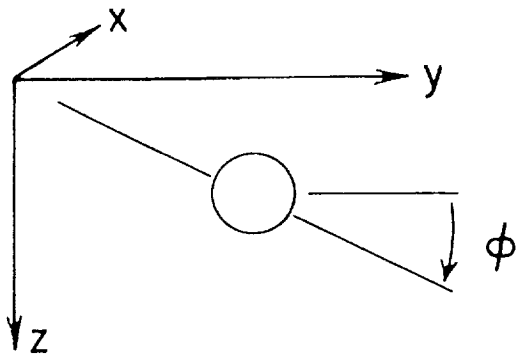

$$\ddot{my} = C_L qS \sin\phi$$

$$\ddot{mz} = - C_L qS \cos\phi + mg(1 - \cos\phi)$$

$$I_{yy}\ddot{\theta} = \left[C_{m_\alpha}\alpha + C_{m_{\dot\alpha}}\frac{\dot\alpha c}{U} + C_{m_q}\frac{\dot\theta c}{U}\right] qSc \qquad (4)$$

$$I_{xx}\ddot{\phi} = C_{\ell_p} qSb \frac{\dot\phi b}{2U} + \zeta_v$$

where

α - angle-of-attack

C_{m_α} - static pitching moment coefficient

$C_{m_{\dot{\alpha}}}$ - dynamic pitching moment coefficient

C_{m_q} - pitch damping coefficient

C_{ℓ_p} - roll damping coefficient

ζ_v - torque generated by vortex

m - aircraft mass

I_{yy} - moment of inertia about x-axis

S - aircraft planform area

q - dynamic pressure

For all dynamic simulations undertaken for the remainder of this report, the characteristics of the encountering aircraft are taken to be that of a Lear jet, and the generator is taken to be that of a 550,000 lb aircraft with a separation distance between vortices taken to be $b = 140$ ft . The Lear jet characteristics are tabulated in Appendix A.

The initial simulation is shown in Figure 7. The Lear jet with controls locked is initially positioned at $Y = Z = 600$ ft and is trimmed to descend and move laterally toward $Y = Z = 0$ at 10 ft/sec. This corresponds to an intercept with the center of the vortex pair at a 3° angle. The upwash of the wake of the 550,000 lb aircraft alters the trajectory of the Lear jet and it passes over the wake and out of the computational domain $|Y| \leq 600$ ft , $|Z| \leq 600$ ft in about 60 seconds. Note that the Lear jet is accelerated to the left during this simulation. To estimate when a rectilinear accelerometer can first detect accelerations which are vortex induced, the above simulation is repeated with the initial position of the Lear jet taken to be at the edge of the computational domain and the aircraft, if trimmed, to move initially inward to $Y = Z = 0$ at 10 ft/sec. Shown in Figure 8 is the location in the computational domain where the magnitude of the lateral acceleration first exceeds $\ddot{y} > 0.1$ ft/sec^2 . Referring back to Table 2c, detecting this level of rectilinear acceleration is well within the state-of-the-art of existing accelerometers.

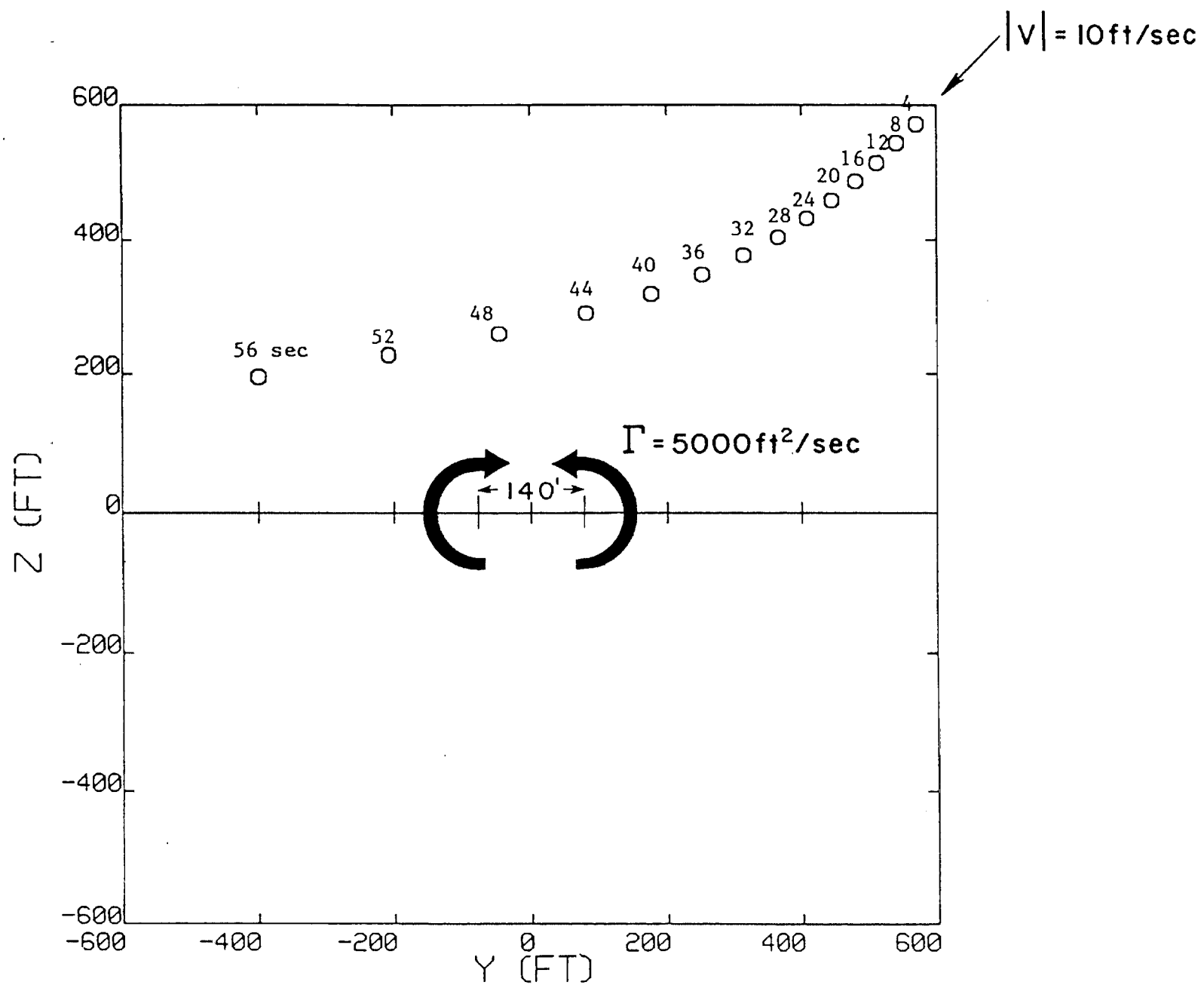

Figure 7. Three-degree-of-freedom simulation controls locked actual Lear jet trajectory.

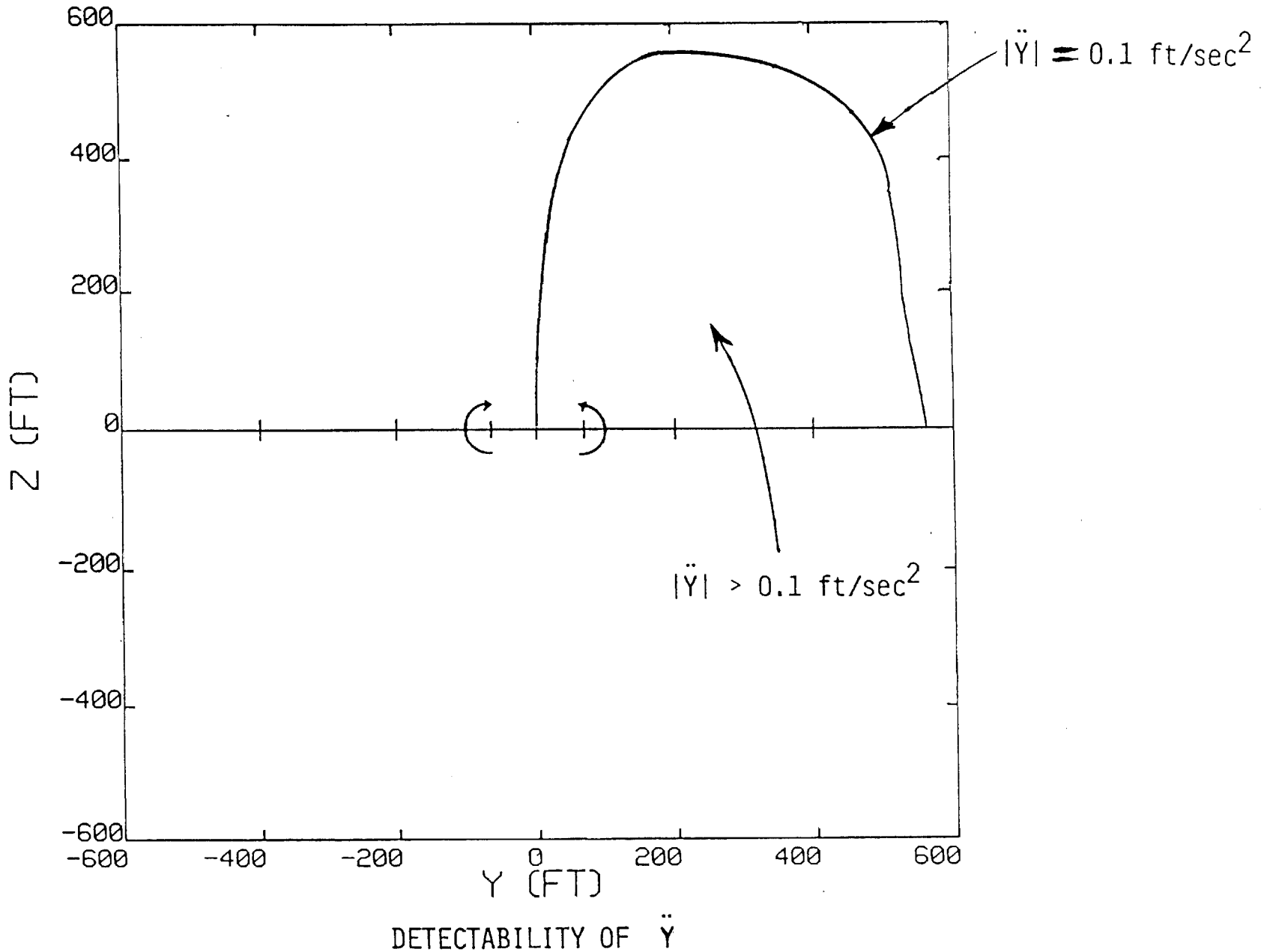

Figure 8. Detection distance using lateral acceleration threshold of 0.1 ft/sec^2 Lear jet encountering aircraft.

The first question which we set out in the Introduction can now be answered.

Question: Using existing instrumentation how far from vortex cores can a vortex signature be detected?

Answer: Existing sensors of the type routinely used on aircraft can detect vortex induced signals several hundred feet away from the center of the wake. The heavier the generating aircraft, the more easily detectable the wake. A wake from a 500,000 lb weight aircraft is detectable at distances of nearly 500 ft from the wake centerline, while the wake of a 100,000 lb aircraft is detectable at a distance of approximately 200 ft from the wake centerline.

3. DETECTORS

The scope of this Phase I study allowed several detector algorithms to receive limited evaluation. This section describes one algorithm which has been selected as a consequence of its conceptual simplicity, and the fact that it is well suited to address signal to noise issues in the next section.

3.1 Detector B - Flow Angle Vanes

If flow angle vanes are mounted on each wing tip known aircraft flight speed it is possible to determine lateral and vertical velocity at each wing tip as a function of time. From these measurements (assuming aircraft transverse motion can be neglected or has been removed from the signals) the following variables can be computed as a function of time.

$$V(t) = \frac{V_r(t) + V_\ell(t)}{2}$$

$$W(t) = \frac{W_r(t) + W_\ell(t)}{2} \qquad (5)$$

$$\frac{\partial W}{\partial Y} = \frac{W_r(t) - W_\ell(t)}{2S}$$

where V , W and $\partial W/\partial Y$ are the lateral velocity, vertical velocity and lateral gradient of vertical velocity, respectively, at the encountering aircraft. The quantity, $2S$, is the distance between the two wing tip flow angle vanes, and subscript r and ℓ denote right and left wing tip sensors, respectively. The left-hand sides of Eq. (5), V , W and $\partial W/\partial Y$, are then equated to their dipole approximations, Eqs. (1) and (3), to yield

$$V(t) = -\frac{\mu}{\pi}\frac{YZ}{R^4}$$

$$W(t) = \frac{\mu}{2\pi}\frac{Y^2 - Z^2}{R^4} \qquad (6)$$

$$\frac{\partial W(t)}{\partial Y} = \frac{\mu}{\pi}\frac{Y(-Y^2 + 3Z^2)}{R^6}$$

It is straightforward but tedious to show that Eq. (6) may be solved for $Y(t)$, $Z(t)$ and μ . Therefore, the position of the encountering aircraft, relative to the center of the wake $(Y(t)$, $Z(t))$, is determined as a function of time, as well as the dipole coefficient or weight of the generating aircraft. The simplicity of this detector is illustrated by writing down the solution for $Y(t)$ and $Z(t)$

$$Y(t) = \frac{2W(t)}{\frac{\partial W}{\partial Y}(t)}\frac{(-1 + 3f^2)}{(1 - f^4)}$$

$$Z(t) = fY(t) \qquad (7)$$

$$f = \frac{W(t)}{V(t)}\left\{1 \pm \sqrt{1 + \left(\frac{V(t)}{W(t)}\right)^2}\right\}$$

and the sign of f must have the same sign of $-V(t)$. Note that the most complicated operation required in this detector algorithm involves taking a square root and, therefore, this detector could easily be programmed into an onboard microprocessor and work in real time. This particular algorithm has been denoted as Detector B internally, and will be called as such for the remainder of this report.

3.2 Detector B - Accuracy

The accuracy of Detector B may be evaluated in several ways. The first is to use the detector to predict the location of an aircraft moving in the wake flow field, and compare this prediction with the actual aircraft location. This comparison is shown on Figure 9 where the predicted positions using Detector B are shown for an aircraft which is actually located on rays originating from the wake centerline $Y = Z = 0$. The flow field used in this study is the same flow field in the simulation shown in Figure 7 (two vortices of strength 5000 ft^2/sec separated by 140 ft). Note that as the vortices are approached, the predicted positions differ from the actual position. This, of course, is a consequence of the fact that our detector is looking for a dipole. The excellent agreement at distances greater than about 100 ft from the wake centerline for such a simple detector algorithm is very encouraging.

A second comparison of algorithm accuracy can be made by recomputing the dynamic simulation of the Lear jet with controls locked, as shown in Figure 7. Removing aircraft motion from the flow angle vane signal (which is easily done here, since aircraft absolute motion is computed) the actual and predicted trajectories are shown in Figure 10. Note that only as the Lear jet position approaches the center of the vortex pair, at a distance of the order of the vortex separation, does the predicted trajectory differ from the actual trajectory. This result is also very encouraging.

The second question can now be answered.

Question: Can this signature be used to compute location of a vortex wake?

Answer: It has been demonstrated that a relatively simple detector algorithm can be used to compute the relative position between an encountering aircraft and a vortex wake. Other algorithms are possible which use both flow vanes and aircraft response variables and detailed analysis of these are a major portion of the Phase II effort.

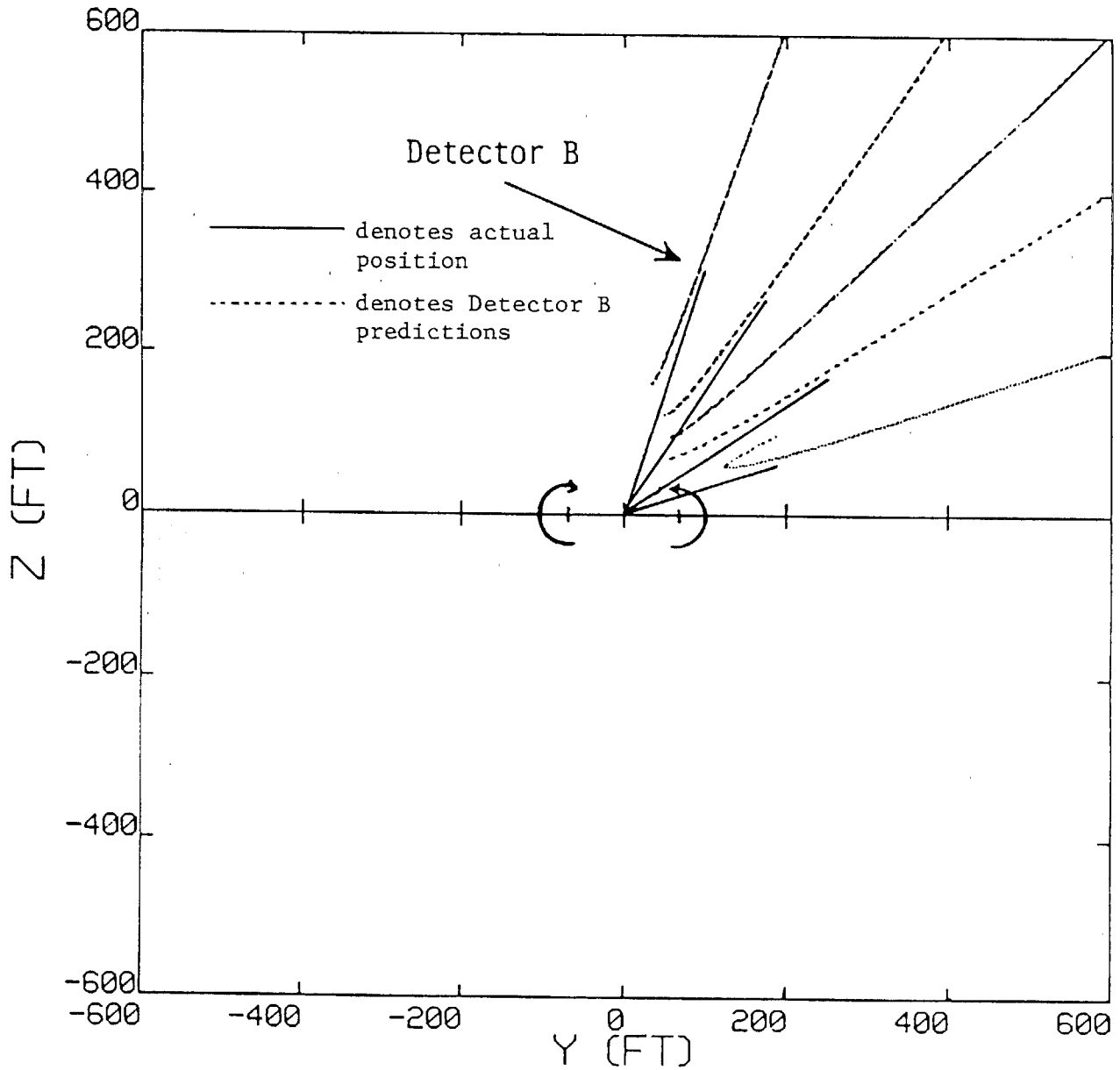

Figure 9. Detector B predicted and actual trajectories for an aircraft located on trajectories which are rays.

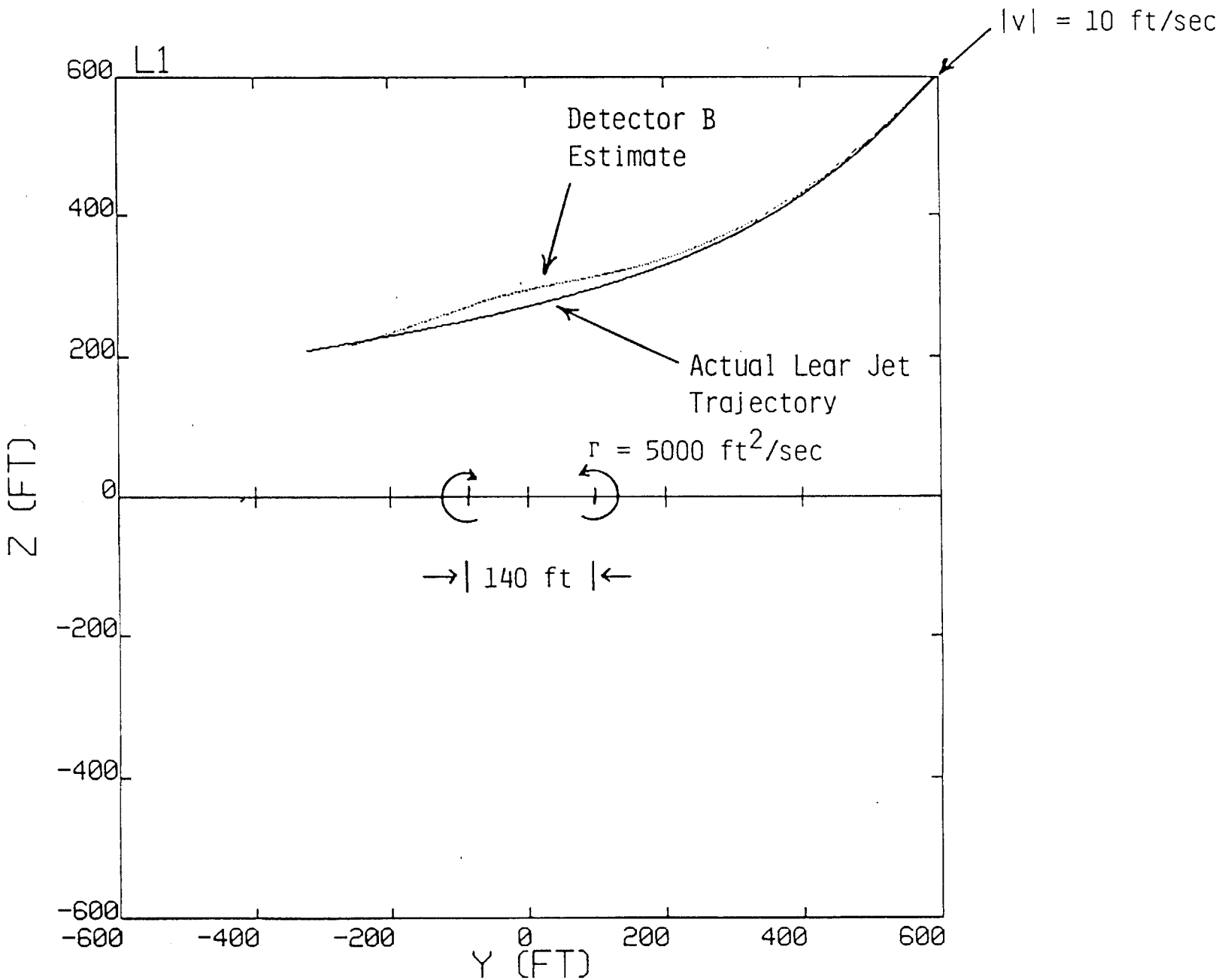

Figure 10. Three-degree-of-freedom simulation controls locked.

3.3 Signal Averaging

In preparation for the next section, which will examine noise, an estimate is made here which determines how significantly detector accuracy decreases when the signal is averaged. Specifically, the predicted aircraft position will be computed from

$$Y_a(t) = \frac{1}{T}\int_{t-T}^{t} Y(t)dt$$

$$Z_a(t) = \frac{1}{T}\int_{t-T}^{t} Z(t)dt \qquad (8)$$

where T is the averaging time and Y_a and Z_a are the averaged predicted aircraft position. The simulation of the Lear jet with controls locked as shown in Figures 7 and 10 is repeated, and the detector position time histories $Y(t)$ and $Z(t)$ are averaged for $T = 4$ and 10 seconds on Figures 11 and 12. A comparison of Figure 7 of actual Lear jet position with that of Figures 11 and 12 suggests that four-second averaging of the detector signal results in errors over the simulation of 75 ft or less, and the ten-second averaging results in errors of hundreds of feet, and is unacceptable. Note that near the end of the simulation from Figure 7, lateral velocities are approaching 50 ft/sec which represents an encounter angle with the wake over 14°. Therefore, it is concluded that with Detector B, and averaging times of the order of four seconds, acceptable predictions of relative positions between wake and aircraft are possible, even with the angle between the wake and encountering aircraft appreciably greater than 6°.

It will be shown in the next section that about four-seconds averaging of the detector signal is sufficient to remove the noise anticipated in the detector signal.

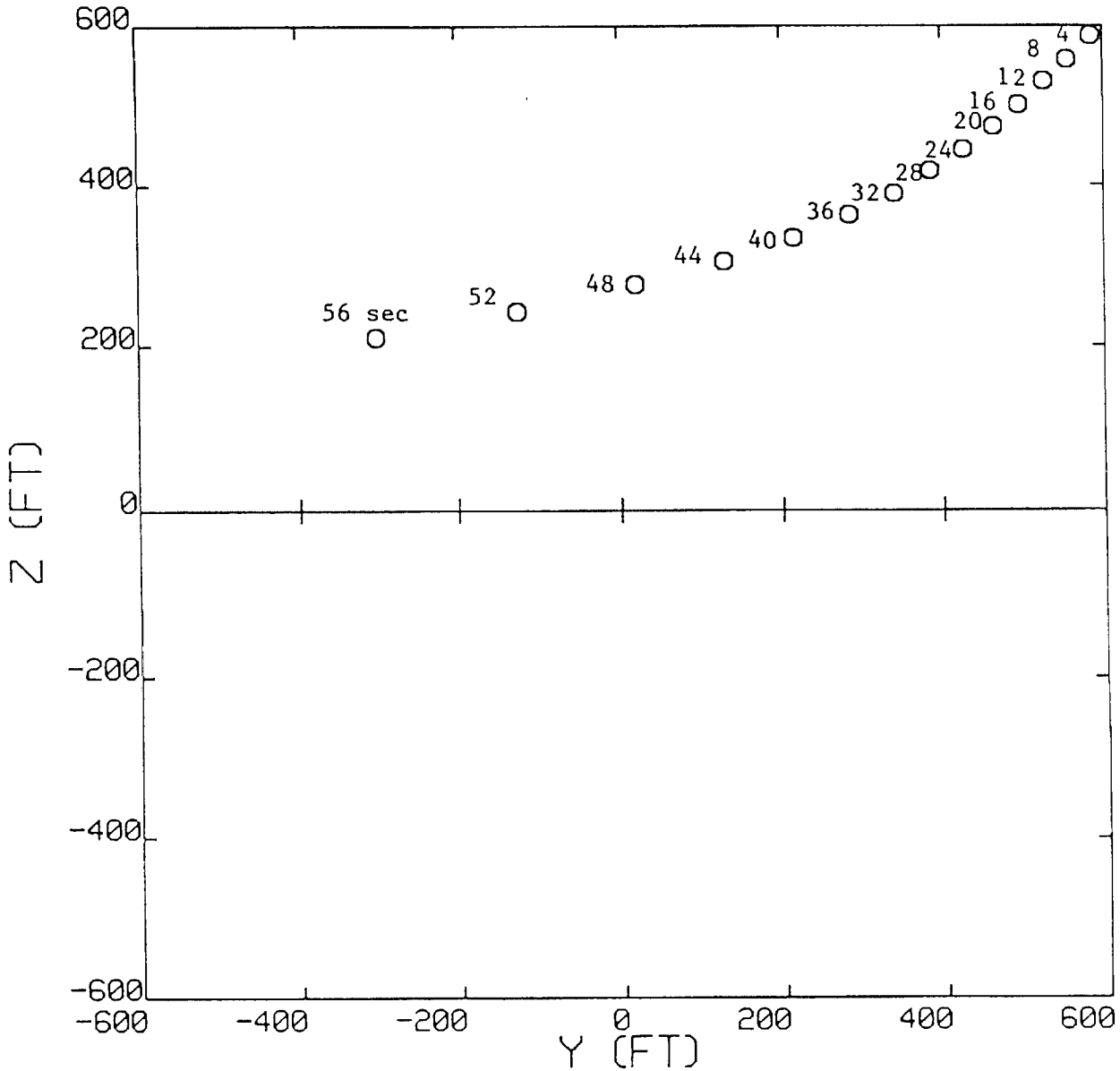

Figure 11. Three-degree-of-freedom simulation controls locked predicted Lear jet trajectory with four-second averaging.

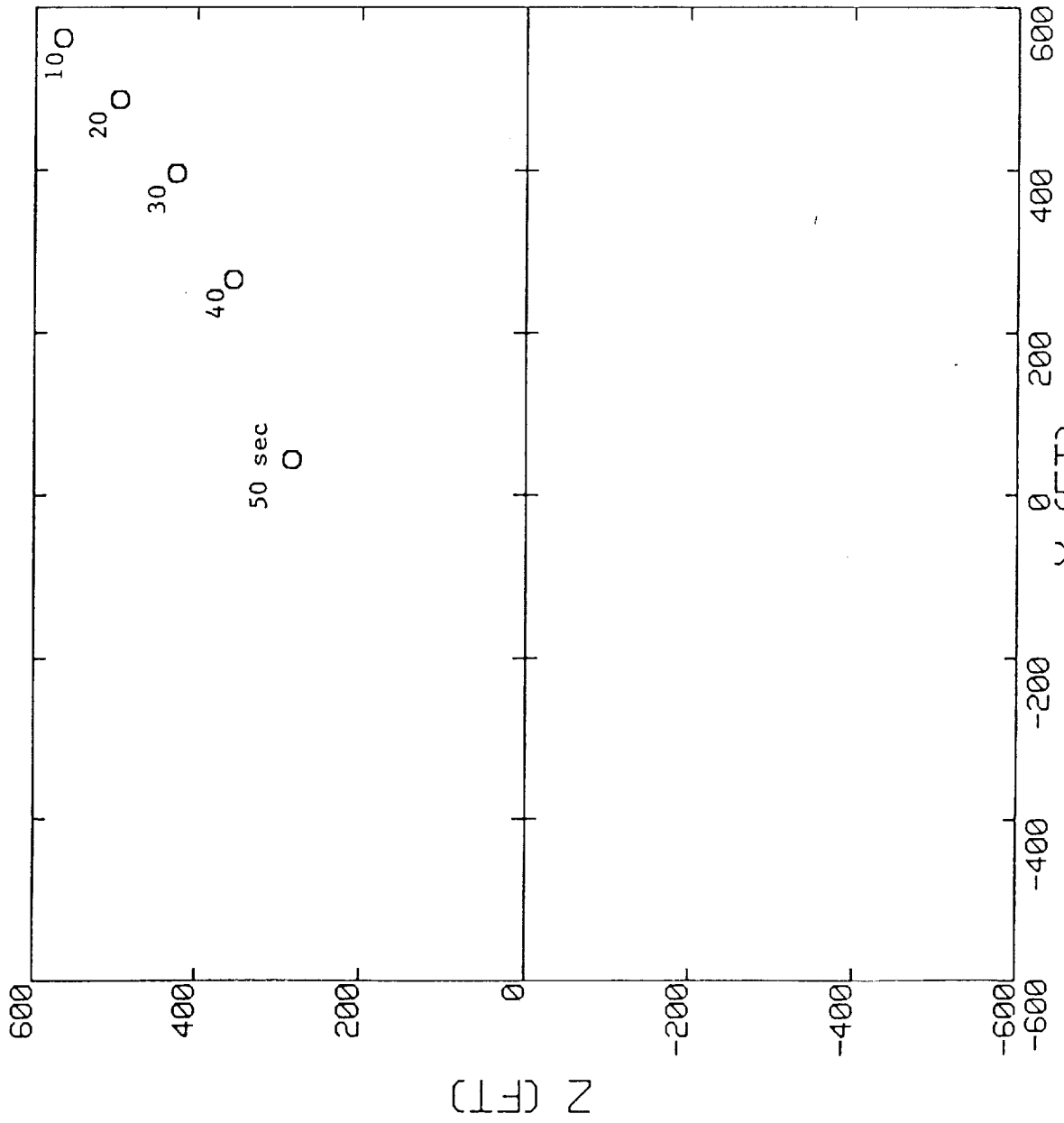

Figure 12. Three-degree-of-freedom simulation controls locked predicted Lear jet trajectory with ten-second averaging.

4. SIGNAL TO NOISE

4.1 Noise Sources

Noise will enter the onboard vortex wake detection signal from:

1) atmospheric turbulence,

2) sinusoidal instability of the wake, and

3) aircraft induced noise from structural flexibility and control surface motion,

as well as from electronic processing of the sensors' output for the sensors under consideration in Section 2.

4.2 Atmospheric Turbulence

Under landing conditions while several hundred feet above the ground, the aircraft is operating in the atmospheric mixed layer. This layer's thickness varies during the day's heating cycle, and is intimately related to the degree of cloud cover among other variables. What is relevant, with regard to operating in a turbulent environment, is that

1) turbulent fluctuations are random (they have no mean when averaged), and

2) turbulent eddies are only correlated over finite distances (over a turbulent integral scale length Λ).

It is also generally agreed that under most conditions in the earth's mixed layer the integral scale or coherence length of eddies is approximately estimated from

$$\Lambda \leq 0.6h \tag{9}$$

where h is the distance above the ground. The idea here is that eddies cannot be bigger than the distance to the nearest solid surface. Here this surface is the earth.

As a rule of thumb, if we wish to average turbulent fluctuations from a signal, the averaging time T_t must be

$$T_t \approx \Lambda/U \tag{10}$$

where U is the flight speed. Recalling that approximately four seconds is available for signal averaging, and using a 200 ft/sec approach speed, noise from turbulence can be removed from the detector's signal at altitudes between

$$0 \leq h \leq 1200 \text{ ft} \tag{11}$$

Since above this altitude a vortex encounter is not likely to be serious, it seems from this simple analysis that noise from atmospheric turbulence may not be an insurmountable issue.

4.3 Sinusoidal Instability of the Wake

The phenomenon of sinusoidal or Crow instability of a vortex wake is shown in Figure 13. The phenomenon has been extensively studied in the literature (Refs 11-14), and an analysis by Bliss (Ref 15) has shown how the phenomenon is forced by atmospheric turbulence. His analysis has shown that the most unstable wavelengths are of the order of 5 vortex spacings. The instability is shown schematically in Figure 14. To demonstrate that the noise introduced into the detector algorithm by sinusoidal instability can be averaged out, we

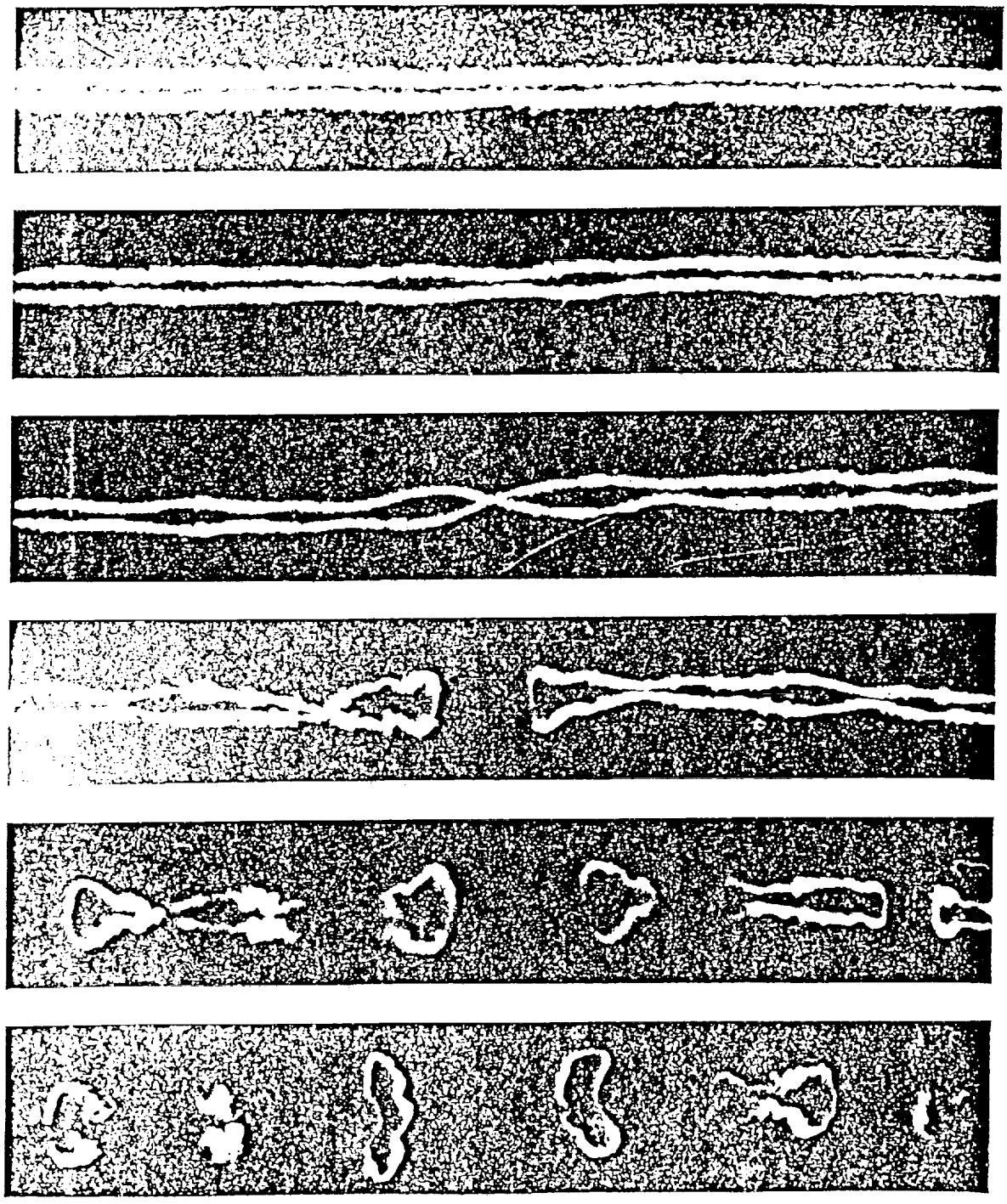

Figure 13. Instability of a pair of trailing vortices. The vortex trail of a B-47 aircraft was photographed directly overhead at intervals of 15 s after its passage. The vortex cores are made visible by condensation of moisture. They slowly recede and draw together in a symmetrical nearly sinusoidal pattern until they connect to form a train of vortex rings. The wake then quickly disintegrates. This is commonly called Crow instability after the researcher who explained its early stages analytically. *Crow 1970, courtesy of Meteorology Research Inc.* (from Ref. 10)

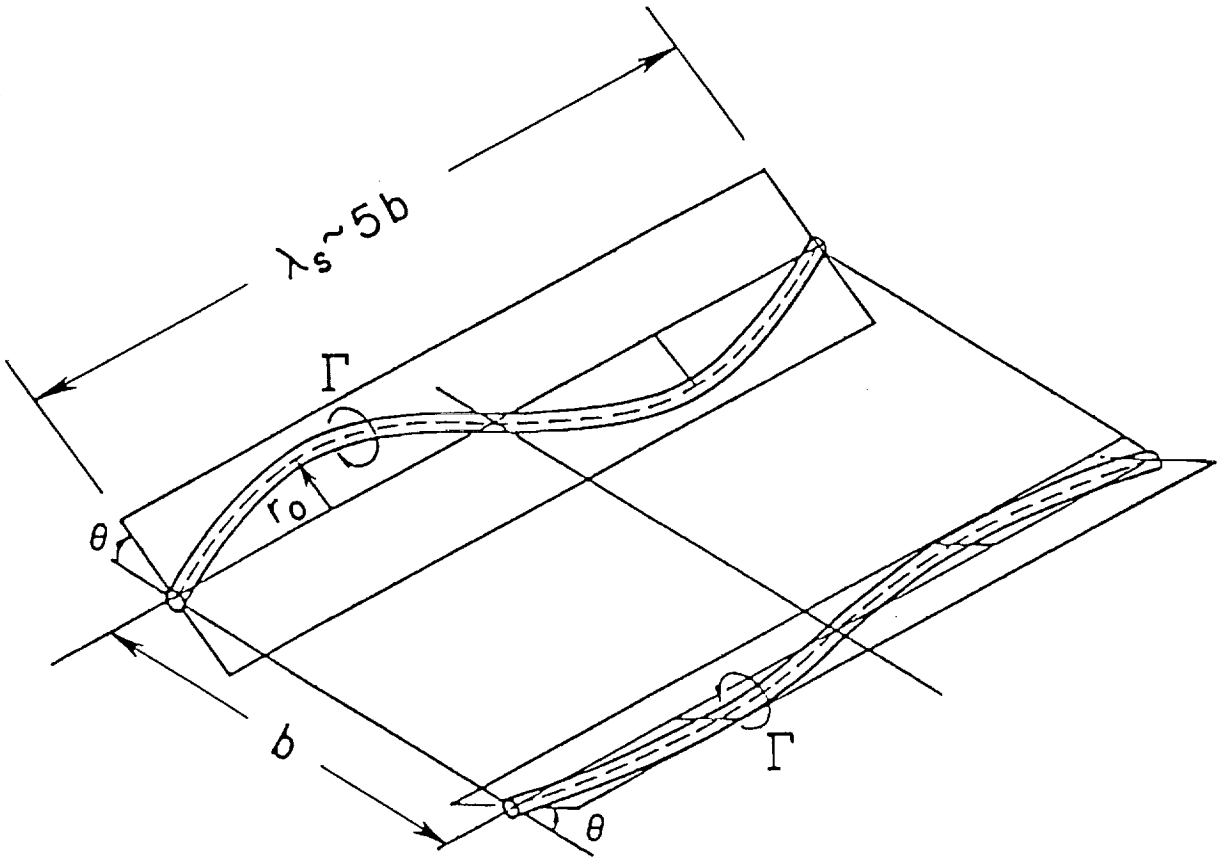

Figure 14. General features of the sinusoidal vortex pair instability. The amplitude of the instability is r_o which grows with time until the vortices link and form crude rings.

have modified the three-degree-of-freedom simulation code velocity field to allow the Lear jet to fly into the vortex velocity field of sinusoidally displaced vortices. In Figure 15 is shown the predicted aircraft trajectory from a detector signal which has been averaged over four seconds, when the amplitude of the instability was taken to be 40 ft, and has a wavelength of 750 ft. All other conditions of the simulation are the same as the simulation shown on Figure 7. It appears again that if four-second averaging of the detector's signal can be achieved in flight, then the noise associated with sinusoidal instability can be successfully removed from the signal. This does not come as a surprise, since the rule of thumb time to average out the sinusoidal instability noise is

$$T_s = \lambda_s / U \qquad (12)$$

or for the conditions used here $T_s \simeq 3.75$ seconds which is less than the four seconds used.

A final comment on sinusoidal instability is relevant here. It is known that as the turbulent intensity increases in the atmosphere, the time at which the vortices link to form rings (as shown in Figure 13) decreases. Bliss (Ref 15) has obtained an approximate expression to evaluate wake time, or time to link. We have computed the wake lifetime for a Lear jet and a B-747 aircraft and the results are plotted on Figure 16. The ordinate is the root mean square vertical turbulent velocity in ft/sec. It is curious that although the detector will have to operate in a noisy turbulent environment, the more turbulent the atmosphere the less likely the wake is a hazard.

4.4 Aircraft Motion

If sensors are mounted at the aircraft's wing tip, or in the aircraft's fuselage as it flies through atmospheric turbulence, wing tip motion and fuselage accelerations will contribute noise to the detection signal. In Appendix B, the details of a two-degree-of-freedom wing flapping model are

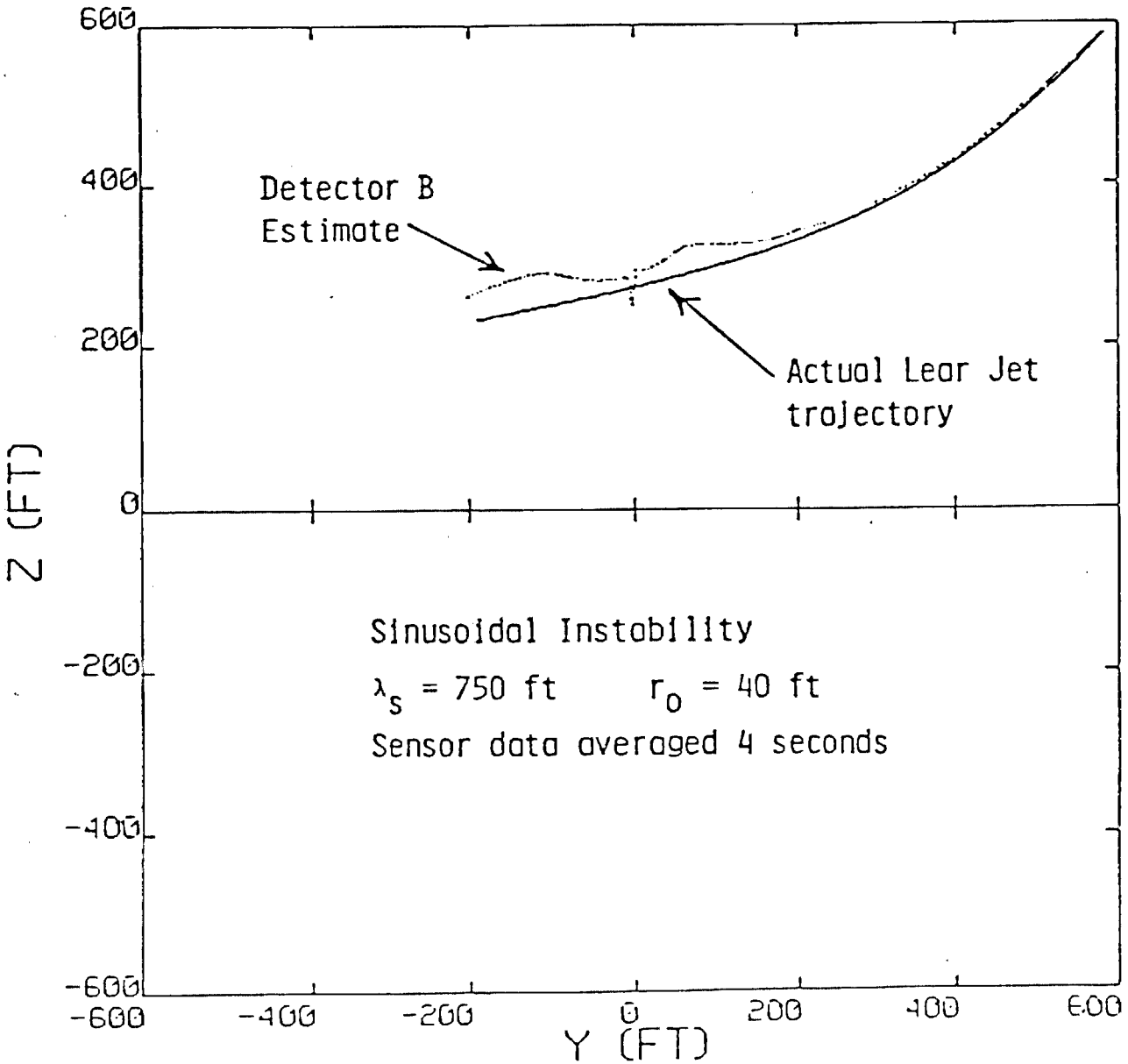

Figure 15. Three-degree-of-freedom simulation controls locked.

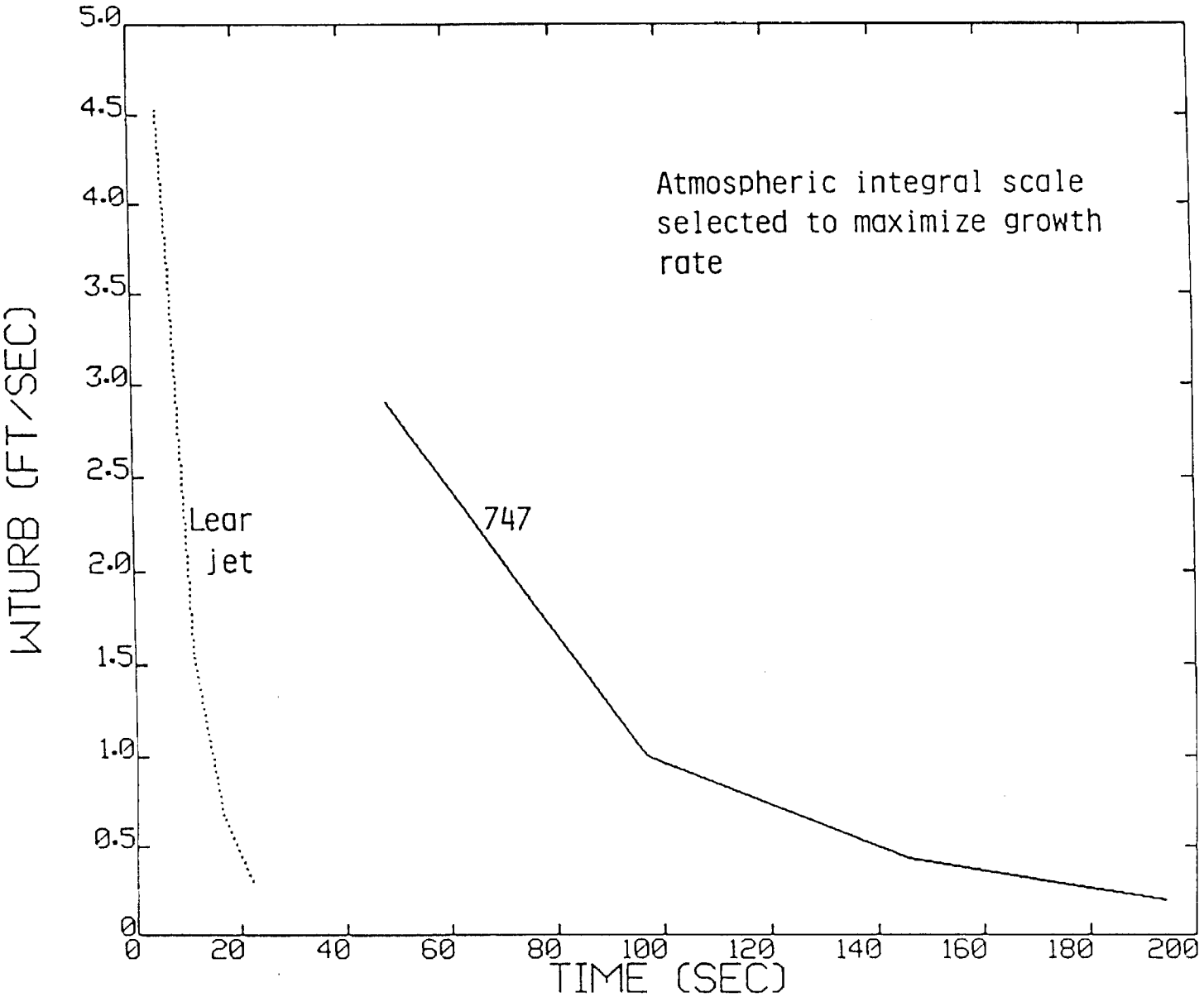

Figure 16. Wake lifetime in a turbulent atmospheric sinusoidal instability.

described. The results from this model are summarized on Figures 17 and 18. From Figure 17, for the aircraft listed on Table 1, nondimensional accelerations of the fuselage are maximum at a turbulence scale of less than 100 ft and are of the order

$$\frac{\ddot{z}}{g} \simeq 7 \frac{\overline{W_t}}{U} \tag{13}$$

where $\bar{W}_t$ is the root mean square vertical turbulent velocity. Using $\bar{W}_t = 1$ ft/sec (mild turbulence), $\ddot{z} \simeq 0.2$ ft/sec^2 is of the order of the threshold value of an accelerometer. This suggests that the noise is of the order of the signal when we first hope to begin detection, but since the scale at which this response occurs is so small, an averaging time of only 100-ft/200-ft/sec = 0.5 sec should be required to remove the noise. A similar conclusion is reached with regard to the root mean square tip velocity $\overline{S\dot{\phi}}$, $\overline{S\dot{\phi}}/\bar{W}_t \sim 0.5$ at a scale of $\Lambda \simeq 100$ ft shown on Figure 18.

The third question can now be answered

Question: How large is the signal to noise?

Answer: At distances at which we wish to begin to detect the presence of a vortex (several hundred feet), the noise will be comparable to the signal. Fortunately, the noise can be removed from the signal by a simple average. Averaging times of the order of four seconds appear to be adequate.

4.5 Detection and Evasion Time

The last issue to be addressed concerns whether a wake can be detected, a warning given to a pilot and an evasive manuever executed before a significant vortex upset occurs. This question can be addressed by example. Referring to Figure 19, shown schematically is the geometry at encounter which is assumed

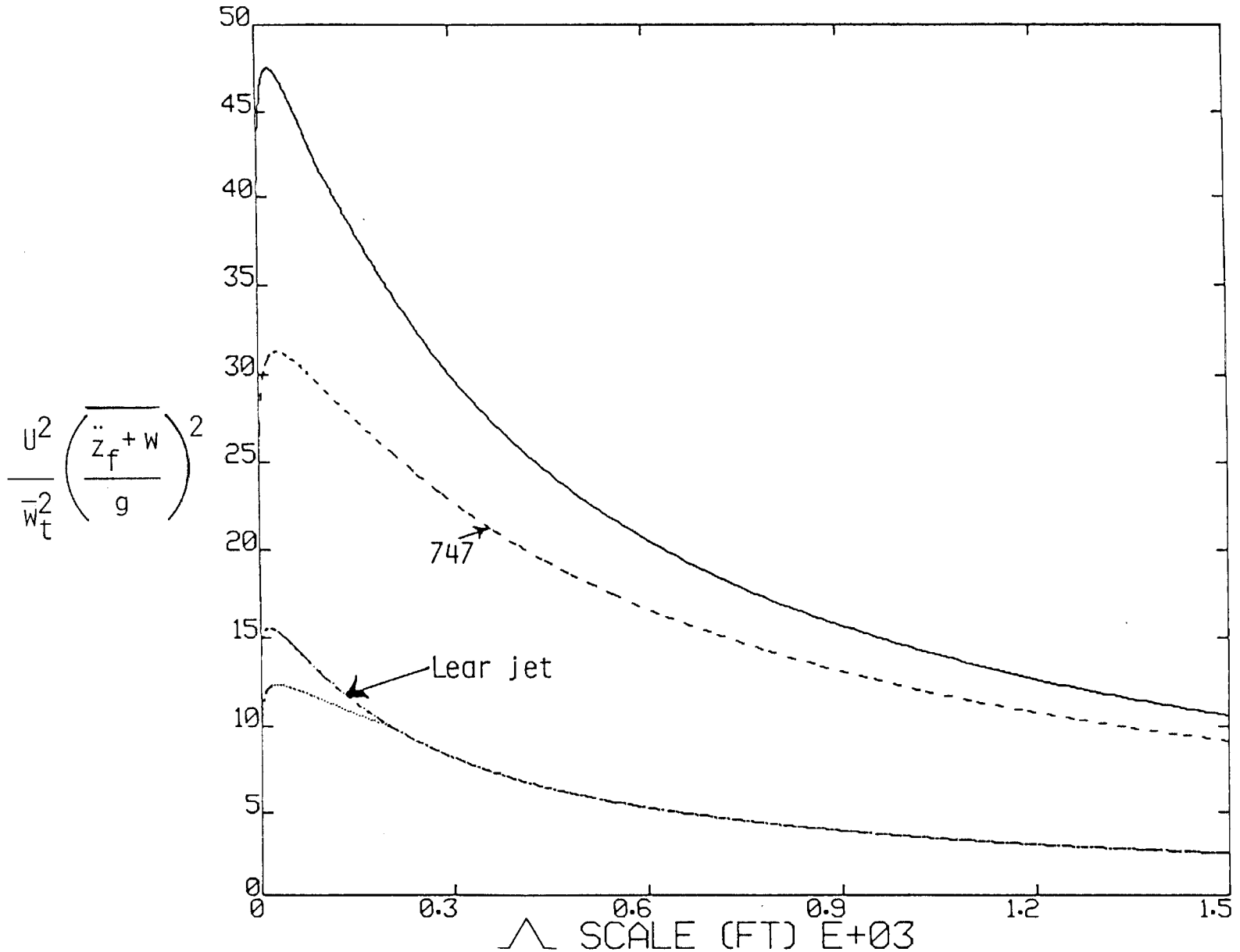

Figure 17. Vertical aircraft acceleration resulting from flying in a turbulent atmosphere.

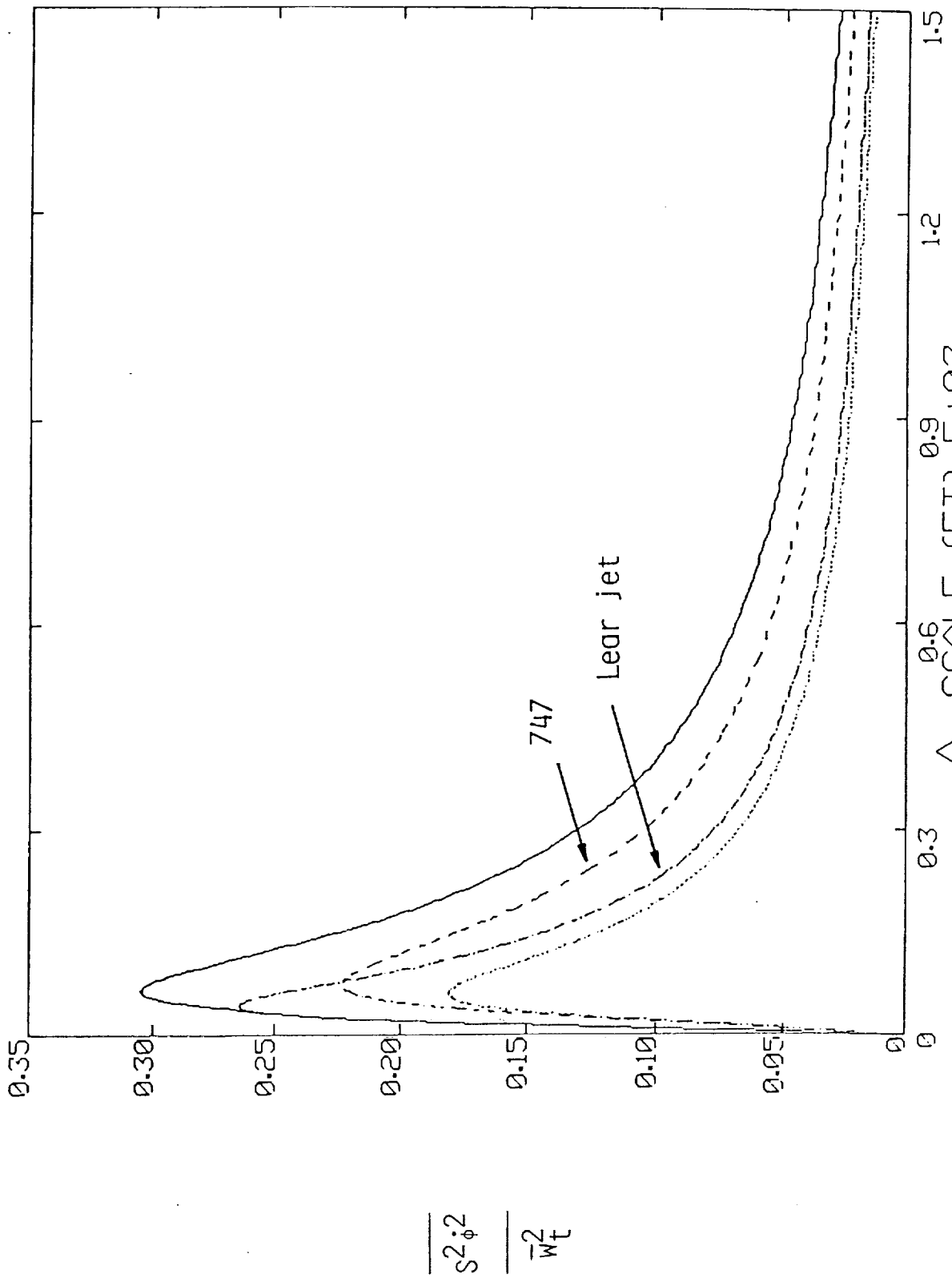

Figure 18. Mean square wing tip velocity resulting from wing bending forced by atmospheric turbulence.

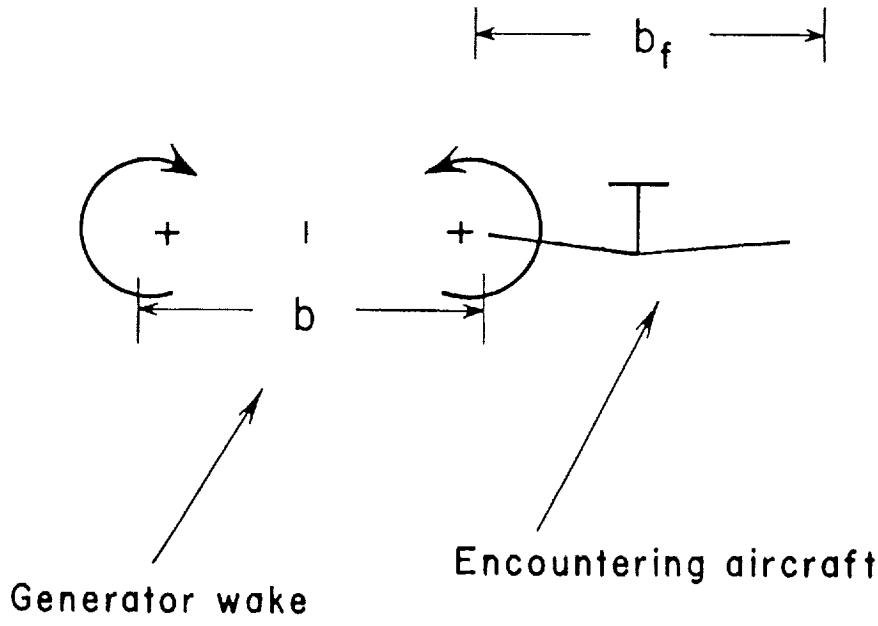

Figure 19. Idealized encounter.

to be the time at which the encountering aircraft's wing tip is coincident with the vortex core. Therefore, the distance at which a detector must begin to detect a vortex is

$$R = \frac{b + b_f}{2} + V_e(T + T_e) \qquad (14)$$

where

b_f is the span of the encountering aircraft

V_e is the lateral encounter velocity (10 ft/sec for a 3° encounter angle)

T is the detector averaging time, approximately four seconds

T_e is the pilot response time to execute an evasive manuever after warning, approximately three seconds

Assuming

$b = 75$ ft

$b_f = 100$ ft

$V_e = 20$ ft/sec (a 6° encounter)

$T + T_e = 7$ seconds

the wake must first be detected at a distance $R = 250$ ft. In light of the detection distance estimates made in Section 2, this detection requirement seems achievable.

The fourth question can now be answered

Question: Will this signal be adequate to provide detection and evasion time for in trail encounter?

Answer: Detectors using existing sensors appear to have sufficient thresholds and accuracy to detect a vortex and provide a pilot with a warning prior to significant vortex upset even with encounter angles of up to 6°.

For encounter angles greater than 6°, it is shown in Appendix C that maximum induced roll rates are well below the roll control authority of the encountering aircraft.

The final question

Question: Are there any other reasons why the proposed concept might not work?

Answer: We have examined the effect of aileron deflection on flow angle vanes mounted on wing tips. This induced noise is small. To date, we have not identified any technical reason why the proposed concept might not work.

5. CONCLUSIONS

The Phase I effort examined the technical feasibility of developing an onboard vortex avoidance system which would utilize existing sensor/instrumentation technology. The following conclusions were reached.

1) Generating aircraft leave as a wake a dipole velocity field which can be detected using state-of-the-art instrumentation.

2) The dipole velocity field itself, or aircraft motions such as roll and/or acceleration, may be sensed to determine the position of the vortex wake relative to the aircraft.

3) A vortex wake of the large jumbo jet may be sensed at lateral distances of the order of 500 ft using existing state-of-the-art instrumentation.

4) Assuming lateral encounter velocities, corresponding to wake interception angles of up to 6°, sufficient time exists to detect the vortex wake, alert the pilot and undertake an evasive maneuver prior to encounter. For encountering angles greater than 6° induced roll rates are below the roll control authority of the aircraft.

5) Instrumentation noise will be an issue and will lead to detection false alarms if not properly accounted for. All indications suggest that noise may be easily removed from the detection signal.

6) While no detection algorithm has been developed or proposed in the Phase I study, it has been shown how two simple flow angle vanes may be used to determine the position of an aircraft relative to a vortex wake.

7) There appears at this time, no technical reason why an onboard vortex avoidance system cannot be developed using state-of-the-art instrumentation.

6. REFERENCES

1. Swedish, W.J.: "Evaluation of the Potential for Reducing Longitudinal Spacing on Final Approach." Report No. FAA-EM-79-7, MITRE Corporation, August, 1979.

2. Croom, D.R.: "Low-Speed Wind-Tunnel Investigation of Various Segments of Flight Spoilers as Trailing-Vortex-Alleviation Devices on a Transport Aircraft Model." NASA Technical Note No. TN D-8162, March, 1976.

3. Croom, D.R.: "The Development and Use of Spoilers as Vortex Attenuators." Wake Vortex Minimization, a symposium held at Washington D.C., February, 1976, NASA Vol. NASA SP-409.

4. Patterson, J.C., Hastings, Jr., E.C. and Jordan, Jr., F.L.: "Ground Development and Flight Correlation of the Vortex Attenuating Spline Device." Wake Vortex Minimization, a symposium held at Washington D.C., February, 1976, NASA Vol. NASA SP-409.

5. Ciffone, D.L. and Lonzo, Jr., C.: "Flow Visualization of Vortex Interactions in Multiple Vortex Wakes Behind Aircraft." NASA Technical Memorandum No. TM X-62,459, June 1975.

6. Corsiglia, V.R. and Dunham, R.E.: "Aircraft Wake-Vortex Minimization by Use of Flaps." Wake Vortex Minimization, a symposium held in Washington, D.C., February, 1976, NASA Vol. NASA SP-409.

7. Aviation Week and Space Technology, March 18, 1985, p. 148.

8. Hallock, J.N. and Eberle, W.R.: "Aircraft Wake Vortices: A State-of-the-Art Review of the United States R&D Program." FAA Report No. FAA-RD-77-23, February, 1977.

9. Holbrook, G.T.: "Vortex Wake Hazard Analysis Including the Effect of the Encountering Wing on the Vortex," Master's Thesis, George Washington University, August 1985.

10. Crow, S.C., AIAA Journal, Vol. 8, pp. 2172-2179 (photo as published in "An Album of Fluid Motion," Stanford University, Parabolic Press, 1982, p. 69).

11. Bilanin, A.J. and Widnall, S.E.: "Aircraft Wake Dissipation by Sinusoidal Instability and Vortex Breakdown." AIAA Paper No. 73-107, presented at the 11th Aerospace Sciences Meeting, Washington, D.C., January, 1973.

12. Crow, S.C.: "Stability Theory for a Pair of Trailing Vortices." AIAA Journal, Vol. 8, December, 1970.

13. Widnall, S.E., Bliss, D.B. and Zalay, A.: "Theoretical and Experimental Study of the Stability of a Vortex Pair," Aircraft Wake Turbulence and Its Detection, edited by Olsen, J., Goldberg, A. and Rogers, M., Plenum Press, New York, 1971.

14. Hackett, J.E. and Evans, P.F.: "Numerical Studies of Three-Dimensional Breakdown in Trailing Vortex Wakes," Journal of Aircraft, Vol. 14(11), November, 1977.

15. Bliss, D.B.: "Effect of Unsteady Forcing on the Sinusoidal Instability of Vortex Wakes," Journal of Aircraft, Vol. 19(9), September, 1982.

APPENDIX A

Lear Jet Characteristics

Weight	10,000	lb
Roll moment of inertia	12,300	$ft\text{-}lb\text{-}sec^2$
Span	34.1	ft
Wing area	231.8	ft^2
Flight speed	200	ft/sec
Lift curve slope	4.69	
Roll damping coefficient	-0.4514	
Aileron roll coefficient	0.23	
Pitch moment of inertia	18,200	$ft\text{-}lb\text{-}sec^2$
Mean wing chord	7.04	ft
Static pitching moment coefficient	-0.974	

APPENDIX B

Two-Degree-of-Freedom Wing Flapping Model

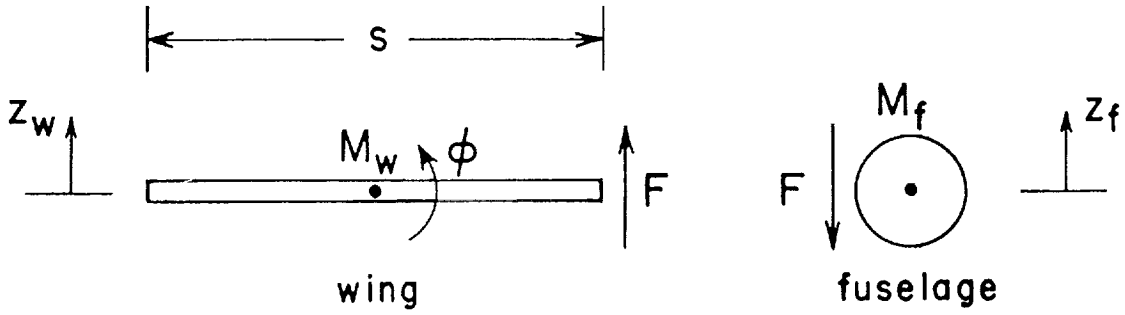

A free body of the wing gives

$$M_w \ddot{Z}_w = F + (W_t - \dot{Z}_w) \frac{1}{2}\rho U C_{L_\alpha} sc \qquad \text{(A-1)}$$

$$I_w \ddot{\phi} = \frac{Fs}{2} - \dot{\phi} \frac{1}{24}\rho U C_{L_\alpha} s^3 c - k\phi \qquad \text{(A-2)}$$

where the second term on the right is the contribution due to integrating the force effect along the wing.

A free body of the fuselage gives

$$M_f \ddot{Z}_f = - F \qquad \text{(A-3)}$$

$$Z_f - Z_w = \phi \frac{s}{2} \qquad \text{(A-4)}$$

In the limit of a large spring force k, the angle ϕ must equal zero to keep the solutions finite. This yields

$$Z_f = Z_w \tag{A-5}$$

$$F = - M_f \ddot{Z}_w \tag{A-6}$$

to give

$$\ddot{Z} + \dot{Z}f = W_t f \tag{A-7}$$

where

$$f = \frac{\frac{1}{2}\rho U C_{L_\alpha} sc}{M_f + M_w} \tag{A-8}$$

The mean square vertical acceleration due to atmospheric turbulence may then be obtained by substituting into

$$\overline{\ddot{Z}^2} = \int_0^\infty \omega^4 S(\omega) \left| H(\omega) \right|^2 d\omega \tag{A-9}$$

where

$$S(\omega) = \frac{L}{\pi U} \overline{W_t^2} \frac{\left(1 + 3\left(\frac{\omega L}{U}\right)^2\right)}{\left(1 + \left(\frac{\omega L}{U}\right)^2\right)^2} \tag{A-10/Ref 1}$$

$$H(\omega) = \frac{f}{-\omega^2 + i\omega f} \tag{A-11}$$

so that

$$\frac{U^2}{W_t^2}\frac{\overline{\ddot{z}^2}}{g^2} = \frac{U^2 f^2}{\pi g^2}\int_o^\infty \omega\left(\frac{\omega L}{U}\right)\frac{\left(1 + 3\left(\frac{\omega L}{U}\right)^2\right)}{\left(1 + \left(\frac{\omega L}{U}\right)^2\right)^2}\frac{d\omega}{(\omega^2 + f^2)} \qquad \text{(A-12)}$$

This equation is plotted in Figure 17 for the aircraft in Table 1 plus the Lear jet.

In the limit of a large fuselage weight M_f, the movement of the fuselage will be suppressed and Z_f must approach zero. This yields

$$Z_w = -\phi\frac{s}{2} \qquad \text{(A-13)}$$

$$F = -M_w\ddot{\phi}\frac{s}{2} - \left(W_t + \phi\frac{s}{2}\right)\frac{1}{2}\rho U C_{L_\alpha} cs \qquad \text{(A-14)}$$

to give

$$\ddot{\phi} + 2\zeta\omega_n\dot{\phi} + \omega_n^2\phi = -\frac{3\zeta\omega_n}{s}W_t \qquad \text{(A-15)}$$

where

$$2\zeta = \frac{C_{L_\alpha} s^3 c\rho U}{6mR^2\omega_n} \qquad \text{(A-16)}$$

$$\omega_n^2 = \frac{k}{mR^2} \qquad \text{(A-17)}$$

The mean square wing tip velocity due to atmospheric turbulence may then be obtained by substituting into

$$\overline{\dot{\phi}^2} = \int_o^\infty \omega^2 S(\omega)\left|H(\omega)\right|^2 d\omega \qquad \text{(A-18)}$$

where, for this equation

$$H(\omega) = \frac{\frac{3}{2}\zeta\omega_n}{-\omega^2 + 2\zeta\omega_n i\omega + \omega_n^2} \qquad \text{(A-19)}$$

so that

(A-20)

$$\frac{s^2\overline{\dot{\phi}^2}}{\overline{W_t^2}} = \frac{9(2\zeta)^2}{4\pi} \int_0^\infty \omega\left(\frac{\omega L}{U}\right) \frac{\left(1 + 3\left(\frac{\omega L}{U}\right)^2\right)}{\left(1 + \left(\frac{\omega L}{U}\right)^2\right)^2} \frac{\omega_n^2 d\omega}{\left(\left(-\omega^2 + \omega_n^2\right)^2 + (2\zeta)^2\omega^2\omega_n^2\right)}$$

This equation is plotted in Figure 18 for the aircraft in Table 1 plus the Lear jet.

Ref: Houbolt, J.C., Steiner, R. and Pratt, K.G.: "Dynamic Response of Airplanes to Atmospheric Turbulence Including Flight Data on Input and Response," NASA Technical Report No. NASA TR R-199, June 1964.

APPENDIX C

Roll Response of an Aircraft Encountering a Vortex Wake

C.1 Literature Review

There is a very large volume of literature dealing with the problem of the dynamic response of one aircraft to an encounter with the wake of another aircraft. The work can be divided into three categories: flight tests to determine the response of an aircraft to another's wake; aerodynamic measurement of the wake characteristics of various aircraft, wind tunnel measurements and theory to estimate the aerodynamic forces and moments induced on an aircraft by the wake of another aircraft; and simulation studies to determine the complete aircraft response as well as the critical handling qualities parameters associated with the response. The latter involve real time models with the pilot-in-the-loop simulations. This section does not attempt to review all of the literature in these areas but rather selects some literature typical of each area for discussion.

Flight test investigations such as references C-1 and C-2 show the severity of the problem. However, the wide variation in the significant parameters associated with the resulting dynamic motions of the aircraft measured during wake encounters makes it difficult to draw very much in the way of quantitative conclusions. Generally, the flight test results of Ref. C-1 where a variety of aircraft were flown through the wake of a C5-A show a decreasing amplitude of the various response variables as the encounter takes place further downstream of the generating aircraft, due apparently to the decay of the trailing vortex system. As would be expected the smaller aircraft show a larger response to the same wake. In general, for encounters of a specific aircraft at a given distance behind the generating aircraft, there is the order of a factor two to three in the range of the maximum roll rate experienced during an encounter. In all instances, the maximum roll acceleration induced by the C5-A on all the test aircraft at least equalled the acceleration generated by full aileron deflection, even when the encountering aircraft was a Convair 990. Reference C-2 shows similar data for

encounters of a B727 wake by a LearJet and a PA-30. The change in peak roll acceleration with downsteam distance in these data are less clear than in Ref. C-1 due to the shorter distances behind the aircraft over which the tests were conducted. Again, in general, the maximum roll acceleration exceeded the control power of the aircraft. References C-1 and C-2 suggest as a criterion for acceptable separation between aircraft that the separation distance should exceed the spacing where the vortex induced acceleration exceeds the roll control power, i.e., the roll acceleration due to full aileron deflection. These experiments were all conducted at relatively high altitude, away from the ground. Reference C-3 mentions that the wake of the C5-A has been observed to rapidly decay and also presents a time history for the roll response of a LearJet to a B727 wake showing a large oscillatory component in the roll acceleration which does not appear in the data of Ref. C-1 and C-2. The source of this oscillatory component, whether due to vortex motion or aircraft flexibility does not seem clear.

Reference C-4, also a series of flight test experiments, shows that if the velocity field through which the aircraft flies is known then the maximum roll acceleration experienced by the aircraft flying through this field can be satisfactorily predicted. The aircraft track, in these experiments, was at an angle of approximately 25° to the vortex centerline in contrast to Ref. C-1 where the pilot attempted to fly along the vortex path until the vortex induced response caused the aircraft to be thrown out of the vortex field. The pilot then attempted to reenter the vortex field. All of these experiments were conducted at relatively high altitude giving sufficient space to recover the aircraft. Variations in the response characteristics shown in Refs. C-1 and C-2 are undoubtedly due to the pilots control actions, as well as the unknown geometry of the encounters and the precise definition of the velocity field as indicated by the results of Ref. C-4. With the possible exception of the maximum roll acceleration, the maximum values of all the other aircraft motion variables would be very sensitive to the precise nature of the encounter, as well as th pilot's control action.

Turning now to the aerodynamic data, and first considering the vortex characteristics as a function of downstream distance, Iverson has shown good correlation for a wide variety of wake data in Ref. C-5, indicating that if

the Reynolds Number based on vortex strength is sufficiently large as would be characteristics of large generating aircraft, the maximum tangential velocity, V_l , and vortex core radius, r_c , vary as

$$V_l = k_1\sqrt{\frac{\Gamma_o U_\infty}{x}} \qquad \text{(C-1)}$$

$$r_c = k_2\sqrt{\frac{\Gamma_o x}{U_\infty}} \qquad \text{(C-2)}$$

Thus, as the distance behind the aircraft (x) increases, the core diameter increases and the maximum tangential velocity decreases. Later it is shown in this section that the response problem can be formulated such that the rolling moment coefficient of the encountering aircraft is expressed directly in terms of core size. Reference C-4 suggests that beyond a certain critical distance downstream, Iverson's correlation is no longer valid and that the tangential velocity decreases more rapidly than the square root of x , and proposes the following proportionality

$$V_l \propto \frac{1}{x^2} \qquad \text{(C-3)}$$

Only a few data points are shown to support this change in character. A large number of data points related to wake characteristics are given by Bofah in Ref. C-12 showing a larger scatter than is indicated by the correlation of Ref. C-5. The experimental wake characteristics presented by Bofah are bounded by laminar and turbulent vortex curves, with the experimental data looking much like transition between these two bounding characteristics. Reference C-4 also indicates that inboard flap deflection on the B747 causes a significant reduction in maximum tangential velocity compared to the undeflected case.

Once the wake flowfield is defined then it should be possible to calculate the rolling moment exerted on an aircraft located in this field. Rossow, in Ref. C-6, has shown that strip theory is quite satisfactory for predicting

the rolling moment induced on a wing in a vortex compared to more elaborate theories if the proper wing lift curve slope is used which accounts for the asymmetrical distribution of lift induced by the vortex. Barrows in Ref. C-7 arrives at a similar strip theory result. Direct correlation of these analytical methods with experimental data seems difficult to find. A number of wind tunnel tests have been conducted to determine the rolling moment on a wing placed in a vortex such as Ref. C-8. Generally, they show results qualitatively similar to what would be obtained from Barrows theory. However, Ref. C-8, for example, shows that a large wing experiences larger rolling moments than a small wing in the same vortex field which is in conflict with the theory given by Barrows. The most likely explanation for the discrepancy is the fact the vortex location is disturbed by the wind tunnel and the presence of the test wing, and the vortex is moving about to such an extent that it is unclear exactly what is being measured. That is, the rolling moment on the wing is a function of time due to the vortex motion with large flucturations, as shown for example in Ref. C-9. In this case, the averaging process will determine the apparent value of the rolling moment on the wing. Experimental data from towing tank tests also presented in Ref. C-8 do not agree with the wind tunnel data and show the opposite trend of rolling moment with wing size compared to the wind tunnel tests.

Simulation studies have been conducted, Ref. C-10, which illustrate the fact that the encounter occurs on a very short time scale, less than one second, as also indicated in the flight tests of Ref. C-3, and show that as far as the pilot is concerned the critical parameter is the bank angle induced by the vortex, and that as the aircraft approaches the ground, the acceptable bank angle becomes quite small especially under IFR conditions. It might be noted that below 500 ft altitude all of the LearJet encounters in Refs. C-1 and C-2 would be unacceptable according to the criteria proposed in Ref. C-10. Other unpiloted simulations or simulations using a paper pilot have been conducted in Ref. C-11. However, a rather complex series of assumptions regarding pilot behavior during a vortex encounter are required that appear difficult to justify from the flight test data. The most complete unpiloted dynamic simulation study is presented by Nelson in Ref. C-13. Nelson's results show clearly the very nonlinear nature of the response problem and clearly illustrate the sensitivity of the vortex induced motion to the initial

flight path of the encountering aircraft relative to the wake of the generating aircraft. Nelson's results appear to be quite well supported by flight test results, described by Condit in Ref. C-12. He shows that in very shallow approaches to the vortex field, if the aircraft is uncontrolled, the outer flowfield tends to drive the aircraft away from the wake and the encounter is quite mild. However, doubling the lateral approach velocity from that corresponding to 3° to 6° changes the encounter from a very mild one to a very severe one in terms of induced bank angle.

Thus, while it is clear that this hazard is a very serious one it appears difficult to precisely quantify the problem. It seems clear that it is a very short term event caused by interaction of an aircraft in a very narrow region of another aircraft wake. Close to the ground under IFR conditions, it appears that almost any encounter is hazardous, except perhaps in the case of one very large aircraft encountering the wake of another very large aircraft.

C.2 Vortex Induced Motions

In this section some basic relationships are given for various quantitities of interest related to the response of an aircraft encountering the trailing vortex of another aircraft. It has been noted in the previous section that it is difficult to precisely quantify this problem, however, some general trends can be pointed out from the analysis. While other aspects of the aircraft response may be important depending upon the circumstances of the encounter, the rolling motion appears most critical and, therefore, this section is primarily concerned with aircraft motion about the roll axis. Unsubscripted values refer to characteristics of the aircraft encountering the vortex and the subscript "g" is used to indicate quantities associated with the wake generating aircraft. For simplicity, only a single line vortex is considered in the following discussion. The roll acceleration of an aircraft can be expressed in terms of the rolling moment coefficient C_ℓ as

$$\dot{p} = \frac{g}{b} \frac{1}{C_L} \left(\frac{b}{k_x}\right)^2 C_\ell \qquad \text{(C-4)}$$

where b is the span of the aircraft encountering the vortex and k_x is the radius of gyration of the aircraft in roll. The ratio of span to radius of gyration is primarily dependent upon the aircraft configuration and an average value of 6.6 characterizes multi-engine aircraft and a value of 10.4 characterizes single engine aircraft. For a given roll moment coefficient, note that the roll acceleration varies inversely as the span of the aircraft. This basic trend with size is due to the fact that for geometrically similar aircraft, the moments of inertia increase faster with size than the aerodynamic moments.

The rolling moment coefficient can be conveniently expressed in terms of the lift coefficient induced at the wing tip of the aircraft encountering the vortex when the aircraft is centered in the vortex and aligned with the vortex axis, C_{LT}, and an effective moment arm, Y_e, measured in spans which depends only upon the taper ratio of the wing and the velocity distribution across the wing due to the vortex flowfield. Thus,

$$C_\ell = C_{LT} Y_e \tag{C-5}$$

where assuming an elliptic loading on the generating aircraft,

$$C_{LT} = a_w \left[\frac{b_g}{b} \frac{U_g}{U} \right] \left[\frac{2}{\pi 2} \frac{C_{L_g}}{AR_g} \right] \tag{C-6}$$

and

$$Y_e = \frac{1}{4} \int_{-1}^{1} \bar{c}\, \bar{\alpha}\, \hat{y}\, d\hat{y} \tag{C-7}$$

where $\hat{y}$ is normalized by the semi-span, the chord is normalized by the average chord based on wing area, and the angle of attack is normalized by the angle of attack induced at the tip. For an untapered wing $\bar{c} = 1$ and an idealized vortex with tangential velocity inversely proportional to radial distance outside the core, and proportional to radial distance inside the core, Y_e is equal to,

$$Y_e = \frac{1}{2}\left(1 - \frac{2}{3}\hat{r}_c\right) \qquad \text{(C-8)}$$

where $\hat{r}_c$ is the core radius in semi-spans. Thus, Y_e varies, by a factor of 3, from 1/2 for an ideal vortex with no core to 1/6 when the core radius is equal to the semi-span of the encountering aircraft wing. It might be noted with this formulation, the primary effect of downstream distance and vortex decay tends to appear as an increasing core radius and consequently a reduction in Y_e. Typically, the core radius is the order of 0.1 span or less for the smallest aircraft considered, the LearJet. The lift curve slope in Eq. (C-6) should be based on a reduced aspect ratio due to the asymmetrical loading produced by the vortex. Rossow shows that using Jones theory gives good agreement with more elaborate methods as well as experimental data. That is,

$$a_w = \frac{2\pi AR}{AR + 6} \qquad \text{(C-9)}$$

The magnitude of the problem can be readily seen by inserting typical values

$$C_{L_g} = 1.4$$

$$AR_g = 6.96$$

$$U_g = U$$

$$AR = 6$$

$$Y_e \simeq 0.4$$

These values give a rolling moment coefficient in terms of span ratio

$$C_\ell = .051\,\frac{b_g}{b} \qquad \text{(C-10)}$$

The severity of the problem can be readily seen given the fact that the maximum available roll control (full aileron deflection) typically varies from .05 (LearJet) to .10 for a wide variety of aircraft (Table C-1) Note that for a LearJet encountering the wake of a B747 the span ratio is about 5.7 indicating a very severe response.

The roll acceleration is of the order of

$$\dot{p} = 1.59 \frac{gb_g}{b^2} \qquad \text{(C-11)}$$

for a multi-engine encountering aircraft at a lift coefficient $C_L = 1.4$.

These calculations indicate maximum values calculated for an aircraft which is centered in a line vortex. Simulator studies of encounters close to the ground indicate that the bank angle of the aircraft induced by the encounter is of concern to the pilot, which implies that the time of the encounter is of importance, as well as the variation of the rolling moment coefficient with displacement of the aircraft away from the vortex centerline. The importance of the bank angle makes the estimation problem much more difficult as it depends on pilot control actions, as well as the precise geometry of the encounter, i.e., the time spent in the center of the vortex, as well as whether the aircraft actually encounters the center of the vortex. As the aircraft is displaced laterally from the center of the vortex, the rolling moment coefficient resulting from the vortex flowfield decreases rapidly, Refs. C-6 and C-7. A similar decrease occurs if the aircraft is displaced vertically. Consequently it can be seen that the spatial region, where the rolling moment exerted on the encountering aircraft is large, is a tube with a diameter of the order of a span of the following aircraft, considering only one single vortex.

If the aircraft flight path is not aligned with the centerline of the vortex, the change in rolling moment with inclination can be calculated. The variation of the rolling moment coefficient depends upon the core size relative to the semi-span of the wing. The variation is contained in the

TABLE C-1

Aircraft	Span (ft)	Roll Control Power (Nondimensional)
B747	195.7	.068
B707	145.8	.080
B727	108	.092
B737	93	.097
DC9	89.4	.067
T37B	33.8	.060
LearJet	34	.047

quantity Y_e and can be expressed as a ratio of the rolling moment coefficient when the aircraft is aligned with the vortex as,

$$\frac{C_\ell}{C_{\ell_{\alpha_i}}} = \left(\frac{1}{\cos^2\alpha_i}\right)\left(\frac{\cos\alpha_i - .667\,\hat{r}_c}{1 - .667\,\hat{r}_c}\right) \qquad \frac{\hat{r}_c}{\cos\alpha_i} < 1 \qquad \text{(C-12)}$$

when the wing is partially within the core and partially outside the core, and

$$\frac{C_\ell}{C_{\ell_{\alpha_i}}} = \left(\frac{1}{\cos^2\alpha_i}\right)\left(\frac{.333\,\hat{r}_c}{1 - .667\,\hat{r}_c}\right) \qquad \frac{\hat{r}_c}{\cos\alpha_i} > 1 \qquad \text{(C-13)}$$

when the wing is entirely within the core. This variation is shown in Figure C-1 for typical core sizes of $\hat{r}_c = 0.1$, $\hat{r}_c = 0.2$. For these core radii typical of the problem of interest it can be seen that for values of ε up to about 45° the rolling moment coefficient varies as $(\cos\alpha_i)^{-1}$, when the aircraft is centered in the vortex and rotated through the angle α_i .

Since handling qualities studies have shown that the critical quantity to the pilot is the bank angle resulting from a vortex encounter, the estimation of the bank angle is now considered. As noted above, in general, it is difficult to estimate the bank angle, due to the larger times involved and the nonlinear nature of the problem as indicated by Nelson's studies. in Ref. C-13. For very shallow approach angles, there may be no encounter at all, thus the trends indicated in the following analysis only apply above some critical encounter inclination. It has been noted that the region in which the induced rolling moment is large is of the order of a semi-span, it seems reasonable to assume that the disturbance to the aircraft can be characterized by a constant rolling moment disturbance acting over the spatial distance of a semi-span, in order to estimate the resulting bank angle. The aircraft traverses this region in a time given by

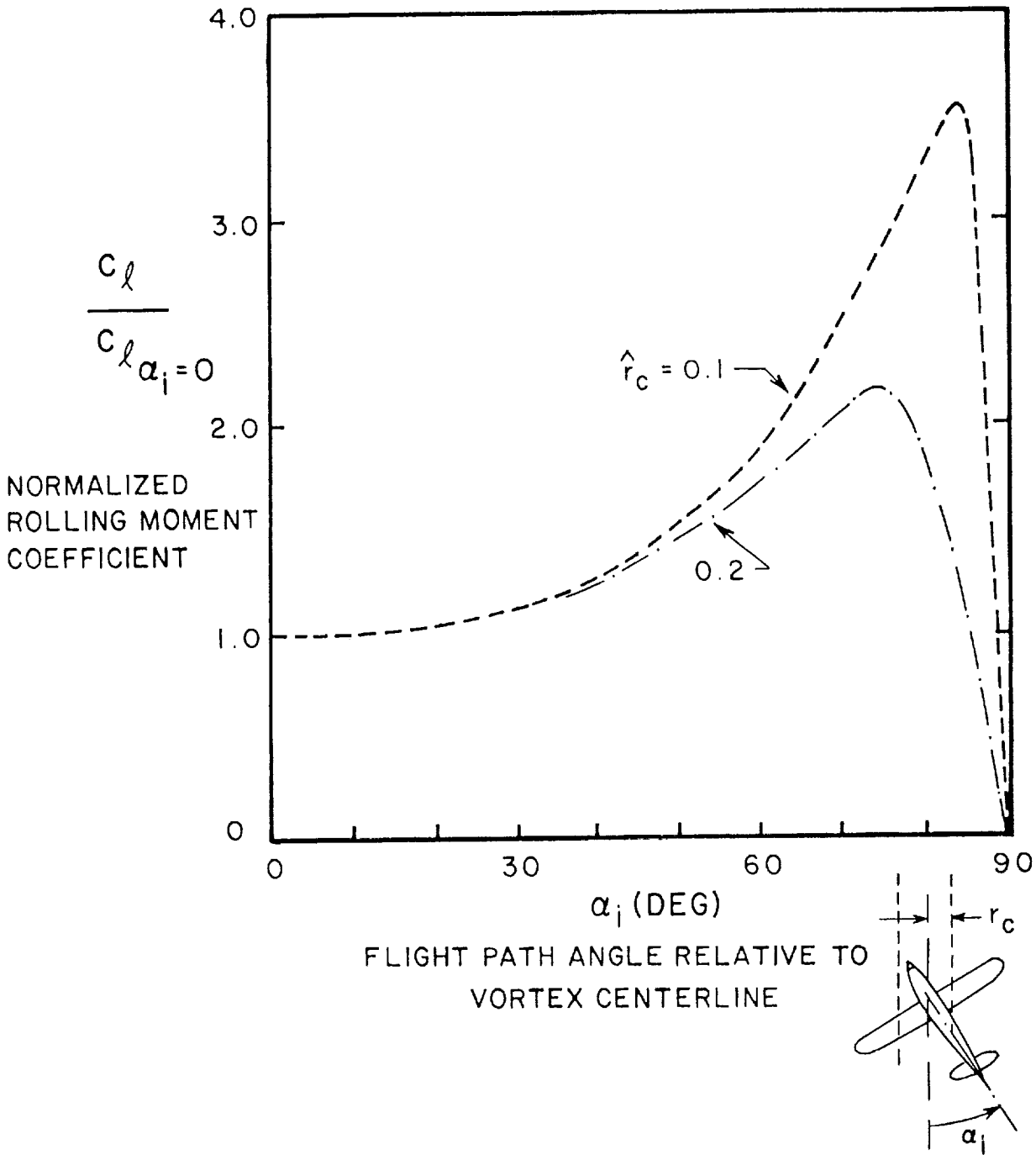

Figure C-1. Variation of maximum bank angle with flight path angle relative to vortex centerline.

$$\Delta t \approx \frac{b}{2U \sin\alpha_i} \qquad \text{(C-14)}$$

This encounter time is typically the order of one second or less (Refs. C-3, C-4 and C-10). This encounter time is usually less than the roll time constant (the inverse of the roll damping derivative) and consequently it is possible to obtain a conservative estimate of the bank angle induced by assuming that the rolling acceleration is constant during this time. Therefore, the bank angle is given approximately by,

$$\Delta\phi \approx \dot{p} \frac{(\Delta t)^2}{2} \qquad \text{(C-15)}$$

In terms of the vehicle parameters

$$\Delta\phi \approx \left(\frac{1}{\pi^2}\right)\left(\frac{1}{C_L}\right)\left(\frac{b}{k_y}\right)^2 a_w \left(\frac{U}{g}\right)\left(\frac{C_L}{AR}\right)\left(\frac{gb}{V^2}\right)\frac{Y_e}{\sin^2\alpha_i} \qquad \text{(C-16)}$$

It is interesting to note that this result is essentially independent of the span of the aircraft that encounter the vortex, with the exception of the influence of core size through the quantity Y_e. This trend is quite different from the result obtained by Tingling in Ref. C-3 for example, who assumes a constant encounter time. If a constant encounter time is assumed then the roll angle will vary as the roll acceleration, and experimental results are presented by Tingling showing that this relationship is not supported by flight test results. The encounter time should depend upon the flight path of the encountering aircraft. Note that for a constant encounter time, the bank angle would vary inversely as the square of the span of the encountering aircraft. It has been assumed in this calculation that the pilot does not respond to the disturbance with control application. The time scale of the encounter increases with increasing aircraft size giving the pilot more time to react and also tending, therefore, to reduce the maximum bank angle. In addition, the maximum rolling moment exerted on the encountering aircraft becomes less relative to the control power of the aircraft and thus any control action is more effective.

Now it is possible to estimate the bank angle induced by a change in incidence of the flight path relative to the vortex. The maximum rolling moment on the aircraft increases as $(\cos\alpha_i)^{-1}$ while the time of the encounter decreases as $(\sin\alpha_i)^{-1}$. Thus, the bank angle induced should vary as $(\sin^2\alpha_i \cos\alpha_i)^{-1}$. Of course, this approach gives an infinite bank angle at $\alpha_i = 0$ since the time of the encounter is infinite. However, as noted above, with no pilot actions there will tend to be no severe encounter below some critical incidence which is difficult to quantify. This is supported both by the flight test results described by Condit, as well as the simulation studies mentioned above. Thus to display the trend the bank angle induced is ratioed to the value induced if the flight path angle is 3° ,

$$\frac{\phi}{\phi_{3^0}} = \frac{\sin^2 3^0 \cos 3^0}{\sin^2\alpha_i \cos\alpha_i} \qquad \text{(C-17)}$$

The variation in bank angle with α_i is shown in Figure C-2. There is a rapid reduction in the maximum bank angle induced as the angle α_i increases. An increase in the incidence angle from 3° to 6° causes a factor of four reduction in the maximum bank angle. The rapid drop off does not indicate that the hazard does not exist for larger encounter angles, but primarily indicates the sensitivity of the bank angle to the geometry of the encounter, and also tends to indicate another reason for the large variations in the flight test data. Below some critical incidence, the bank angle induced will decrease rapidly as the aircraft will not encounter the center of the vortex. These results indicate that the vortex induced bank angle is very sensitive to the precise details of the encounter and thus a reason for the large variability shown in flight test.

These idealized relationships essentially provide upper limits on the roll acceleration and bank angle in an encounter and are difficult to directly verify from flight test data due to the inability to provide precise experimental control and the sensitivity noted above. It has been shown above for example that the bank angle induced is very sensitive to alignment of the aircraft relative to the vortex axis and this is difficult to quantify in a flight test. It has also been assumed that the pilot takes no action where in fact there will be pilot action. The effectiveness of the pilot's response

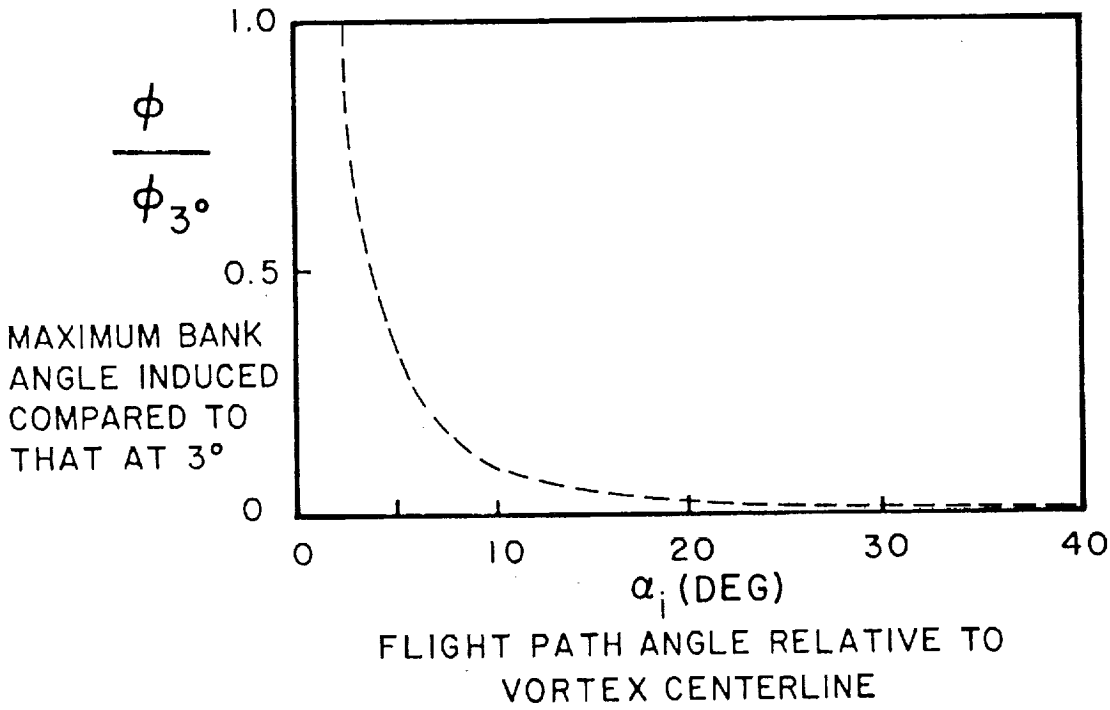

Figure C-2. Variation of rolling moment coefficient with flight path angle relative to vortex centerline as a function of core radius.

will depend upon the time scale of the disturbance and thus the pilot in a larger aircraft is likely to be more effective in countering the disturbance. Furthermore, the roll acceleration induced on the larger aircraft will be smaller as well as the rolling moment coefficient and consequently the roll moment induced by the vortex will be a smaller multiple or fraction of the control power of the aircraft and consequently on a larger aircraft the pilot's action will be more effective in reducing the maximum bank angle that occurs as a result of the disturbance. Thus, even though the simple theory given above indicates that the bank angle induced depends only on the size of the generator aircraft, it is likely that for reasons given above the maximum bank angle experienced will be smaller for larger aircraft encountering the same disturbance.

The general trends indicated by this analysis are supported by the idealized simulation studies of Ref. C-10 where the direct dependence of bank angle induced on encounter angle can be seen to vary in the manner given by the simple result above.

Close to the ground, other aspects of the aircraft motion may also become critical especially under IFR conditions, where any deviations from the glide path are significant. Studies have indicated that normal acceleration, as well as the dutch roll dynamics that ensue after the initial disturbance can be critical factors as well.

C.3 Dynamic Solution (Linear Theory)

It is possible to quantify further the roll response of the encountering aircraft by numerical calculation if the aircraft trajectory is assumed and the vortex flowfield is simplified by assuming that about each vortex the swirling velocity is given by

$$V = \frac{\Gamma_g r}{2\pi(r^2 + r_c^2)} \qquad \text{(C-18)}$$

where r is measured from the center of each vortex.

Since the encounter angle α_i ranges from 0° to 90°, long encounter times are possible and roll damping is included in the equation for roll rate. It is easily shown that

$$\dot{p} + \frac{1}{6}\left(\frac{S}{S_g}\right)\left(\frac{b}{k_x}\right)^2 \frac{C_{L_\alpha}}{C_{L_g}} \frac{g}{U_\infty} p = \frac{C_{L_\alpha}}{2\pi} \frac{gS}{b_g k_x^2} I \qquad \text{(C-19)}$$

where

$$I = -\frac{\sqrt{y_o^2 + r_c^2}}{b}\left[\tan^{-1}\left(\frac{x_o + s\cos\alpha_i}{\sqrt{y_o^2 + r_c^2}}\right) - \tan^{-1}\left(\frac{x_o - s\cos\alpha_i}{\sqrt{y_o^2 + r_c^2}}\right)\right]$$

$$- \frac{x_o}{2b} \ln\left[\frac{(x_o + s\cos\alpha_i)^2 + y_o^2 + r_c^2}{(x_o - s\cos\alpha_i)^2 + y_o^2 + r_c^2}\right] \qquad \text{(C-20)}$$

$$+ \frac{\sqrt{y_o^2 + r_c^2}}{b}\left[\tan^{-1}\left(\frac{x_o + b_g + s\cos\alpha_i}{\sqrt{y_o^2 + r_c^2}}\right) - \tan^{-1}\left(\frac{x_o + b_g - s\cos\alpha_i}{\sqrt{y_o^2 + r_c^2}}\right)\right]$$

$$+ \frac{x_o + b_g}{b} \ln\left[\frac{(x_o + b_g + s\cos\alpha_i)^2 + y_o^2 + r_c^2}{(x_o + b_g - s\cos\alpha_i)^2 + y_o^2 + r_c^2}\right]$$

is the nondimensional torque induced by a vortex pair of spacing b_g. The coordinates used above are shown schematically on Figure C-3. The encounter angle, α_i, is prescribed and results in an encounter velocity, V, by

$$\alpha_i = \sin^{-1}\frac{V}{U_\infty} \qquad \text{(C-21)}$$

All results presented below assume that the encountering aircraft's wings remain level so that the torque may be evaluated from I. Also, the initial position of the encountering aircraft is assumed to be

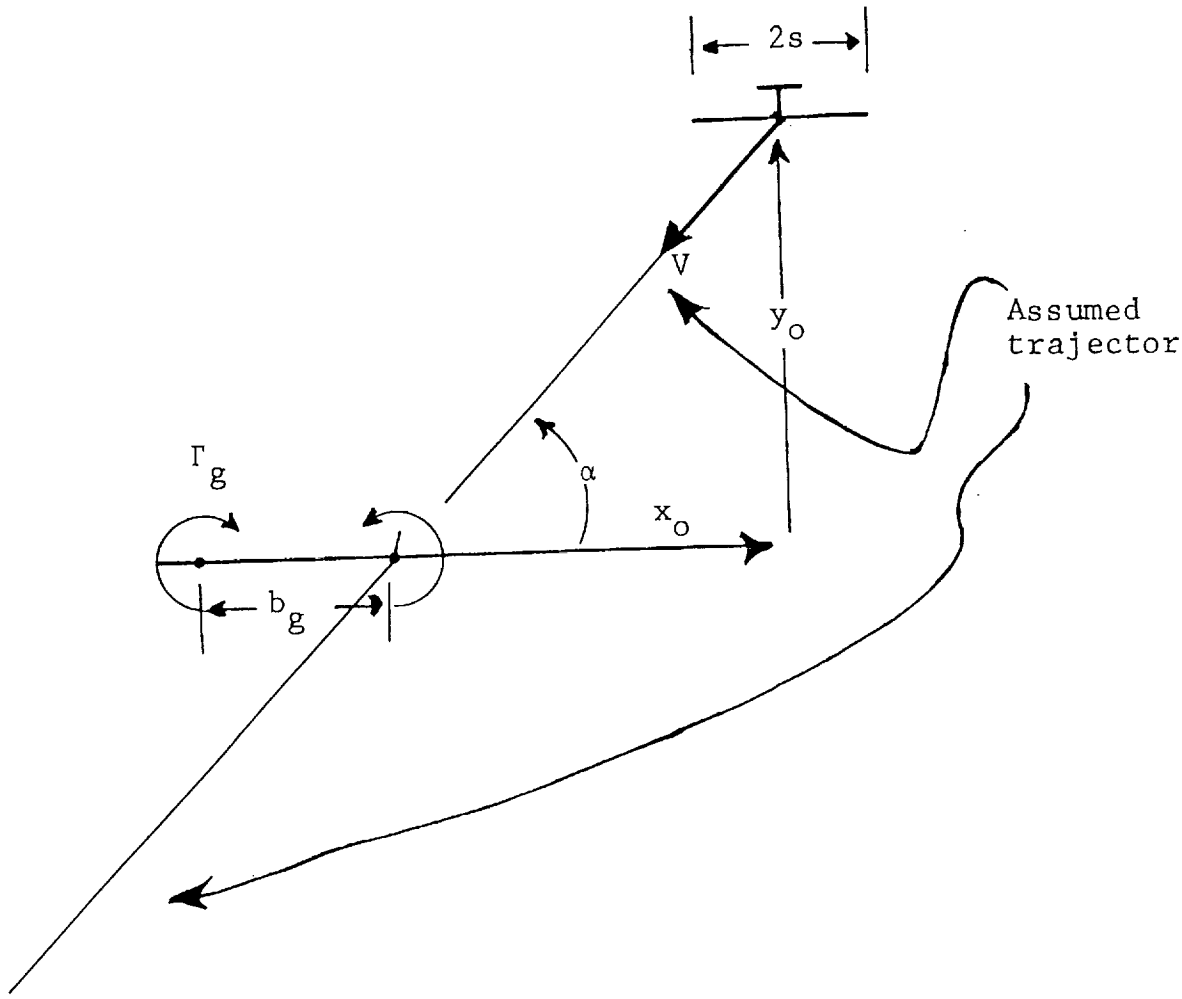

$$\alpha_i = \sin^{-1} \frac{V}{U_\infty}$$

Figure C-3. Assumed encounter geometry. The encountering aircraft trajectory passes through the center of the right vortex along a path which is at angle α from the horizontal.

$$\sqrt{x_o^2 + y_o^2} = 300 \text{ ft} \quad , \quad \alpha = \tan^{-1} \frac{y_o}{x_o} \qquad \text{(C-22)}$$

Results for the maximum roll rate as a function of α_i and α are shown on Figures C-4 - C-7. For the following generator/encounter aircraft

Generator	Encountering Aircraft
B747	B737
B747	DC9
B727	B737
B727	DC9

Note the rapid drop-off of maximum roll rate with encounter angle α_i and the rather weak dependence on trajectory α. This weak dependence is presumably due to the fact that all trajectories pass through the center of the vortex on the right as shown on Figure C-3. Note that the inclusion of roll damping limits all maximum roll rates to

$$\frac{sp}{U_\infty} < 0.2 \qquad \text{(C-23)}$$

which typically is above the roll authority of current transport aircraft. However, an encounter trajectory, as prescribed above, is highly unlikely and would require, if even possible, substantial pilot control inputs. The results presented here should be taken as an upper bound of what might actually occur in practice.

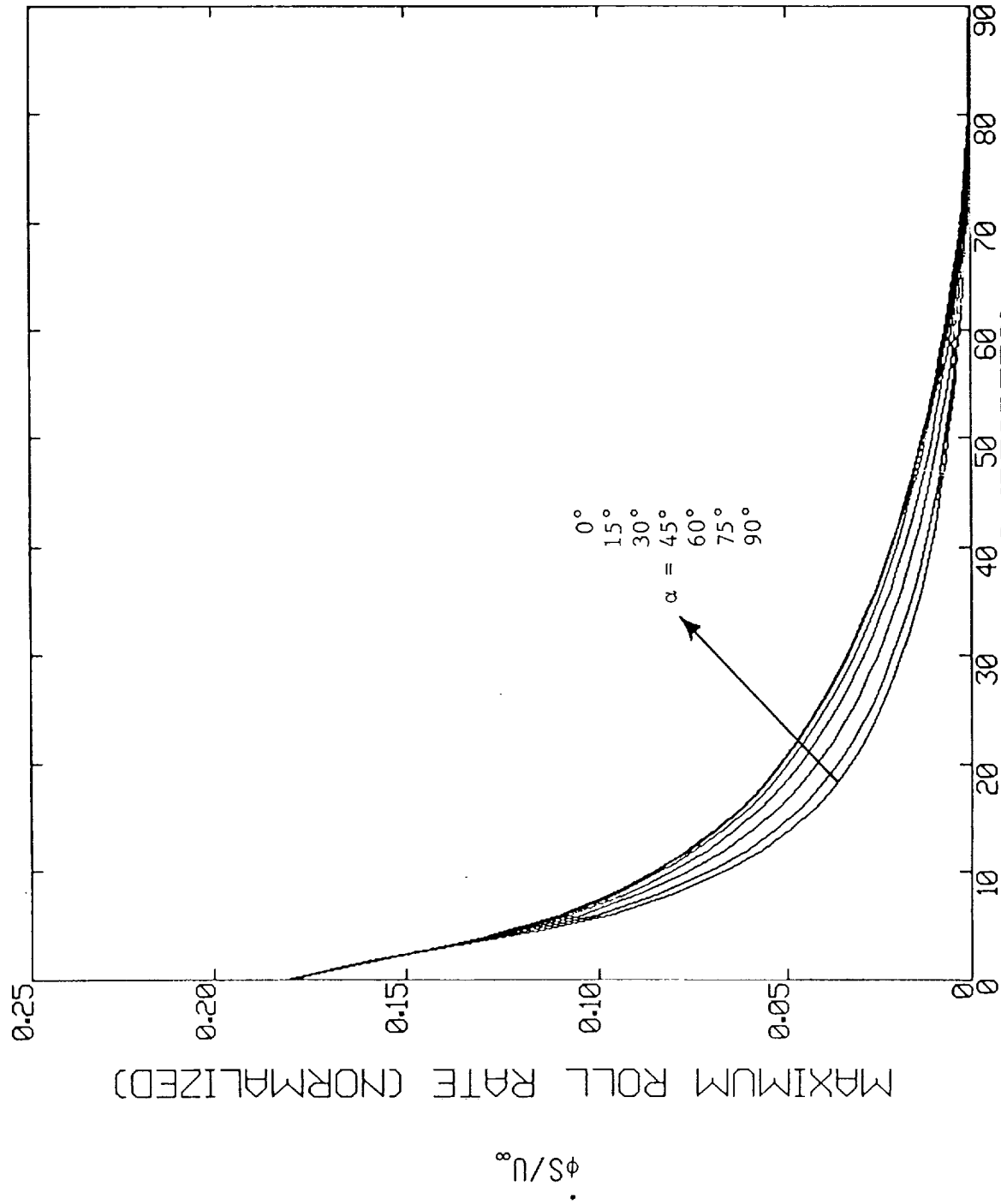

Figure C-4. Maximum roll rate induced on a B737 encountering the wake of a B747.

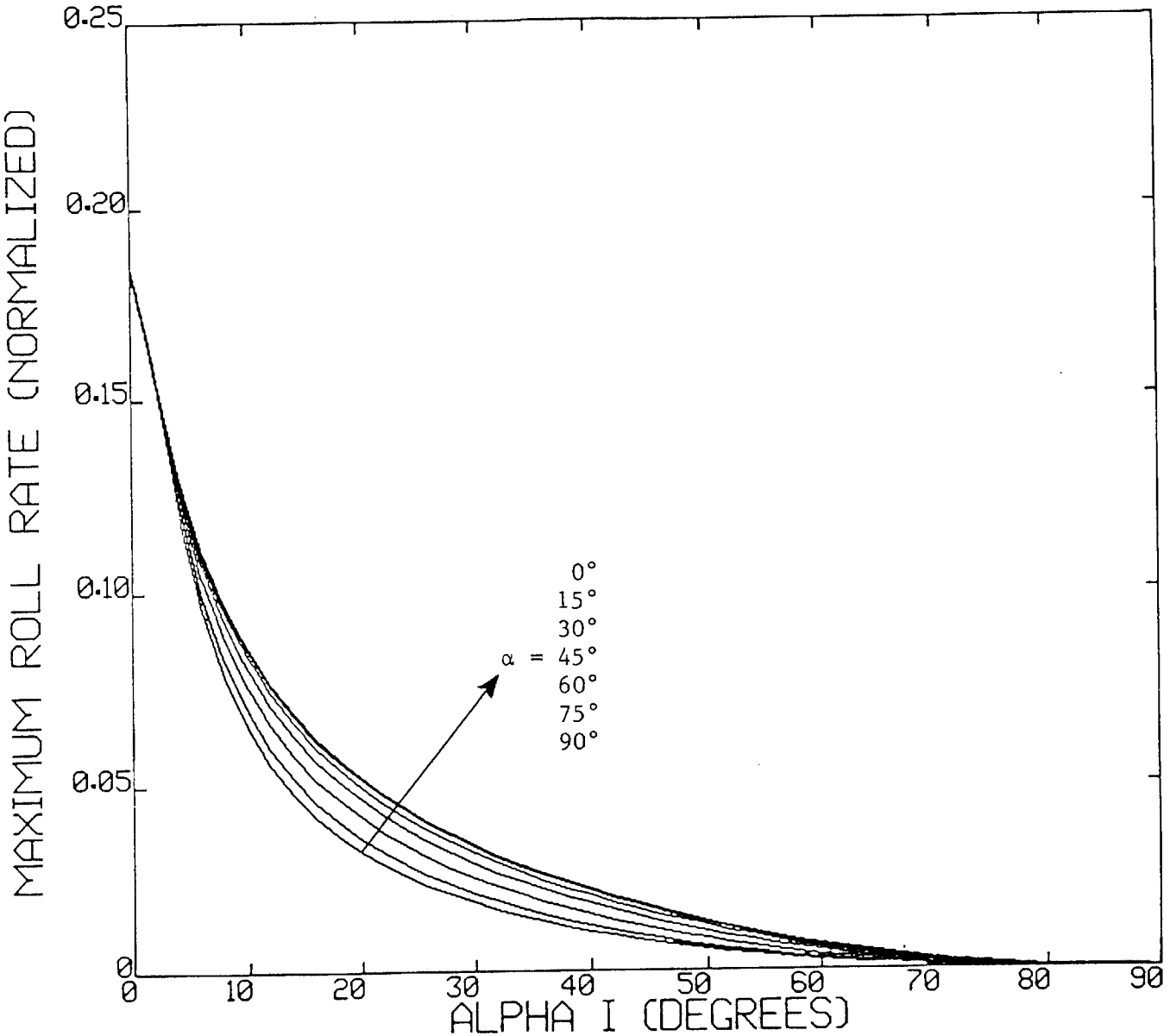

Figure C-5. Maximum roll rate induced on a DC9 encountering the wake of a B747.

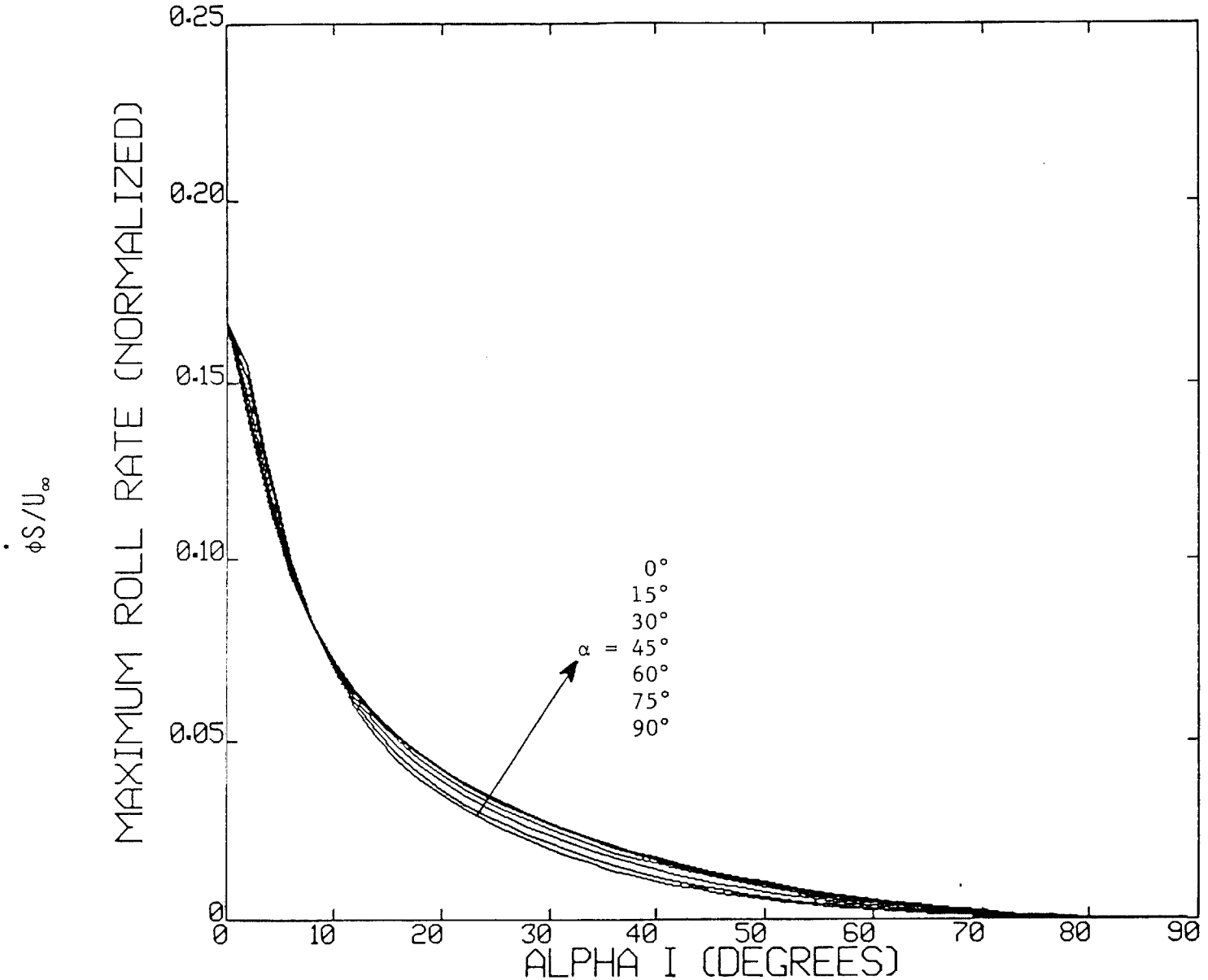

Figure C-6. Maximum roll rate induced on a DC9 encountering the wake of a B727.

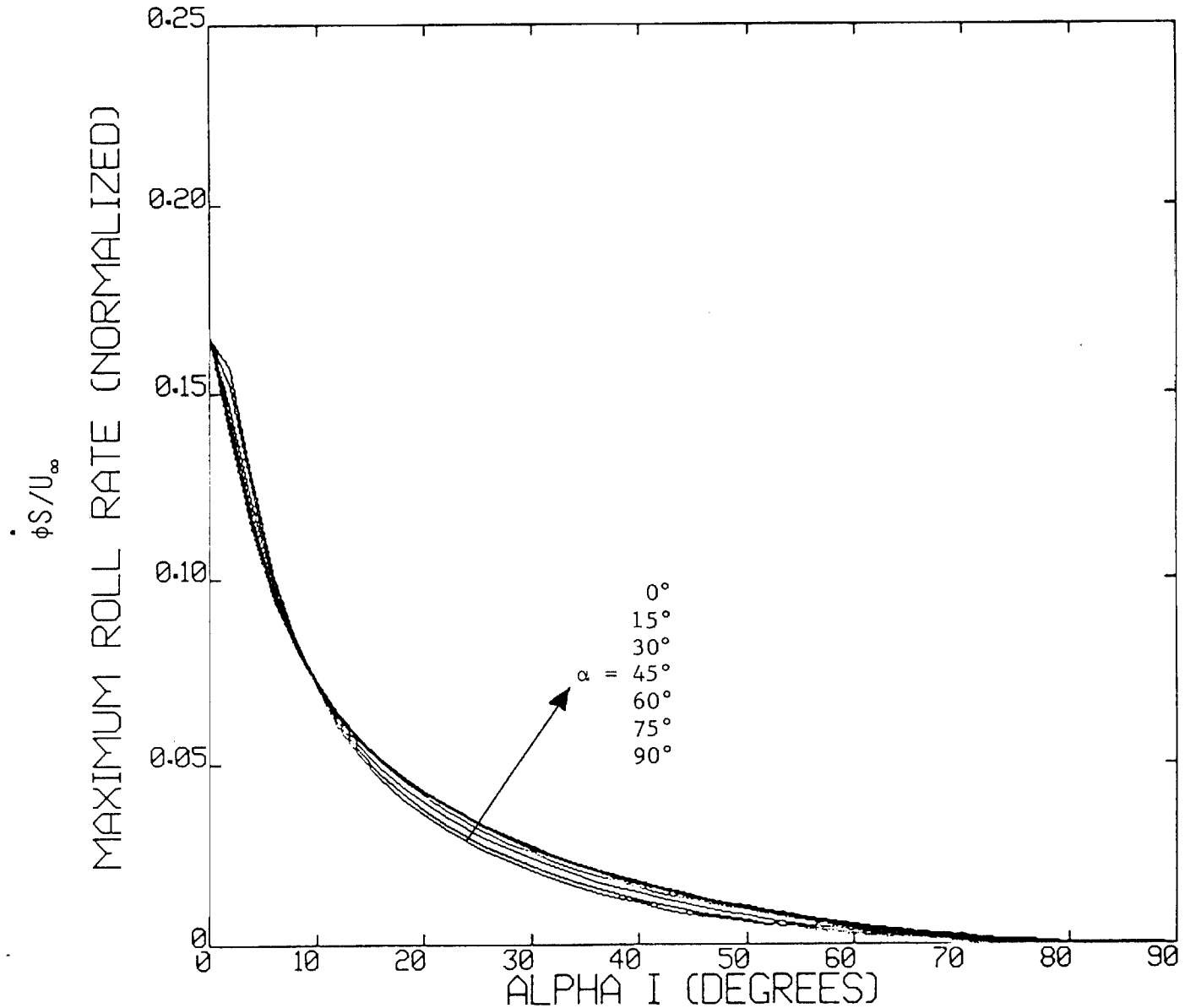

Figure C-7. Maximum roll rate induced on a B737 encountering the wake of a B727.

Appendix C References

C-1. Andrews, W.H. et al "Exploratory Flight Investigation of Aircraft Response to the Wing Vortex Wake Generated by Transport Aircraft," NASA TN D-6655.

C-2. Barker, M.R. et al "Flight Investigation of the Vortex Wake Characteristics Behind a Boeing 727 During Two-Segment and Normal ILS Approaches," NASA TM X-62, 398 (FAA-NA-75-151), January 1973.

C-3. Tingling, B.: "Estimate of Vortex Induced Roll Excursions Based on Flight and Simulation Results," Aircraft Wake Vortices Conference, FAA-RD-77-68.

C-4. Short, B.J. and Jacobsen, R.A.: "Evaluation of Wake Vortex Upset Model Based on Simultaneous Measurements of Wake Velocities and Probe Aircraft Accelerations," NASA TM 78561.

C-5. Iverson, J.A.: "Correlation of Turbulent Trailing Vortex Decay Data," J. Aircraft, Vol. 13, May 1976.

C-6. Wake Vortex Minimization, NASA SP-409.

C-7. Barrows, T.: "Simplified Methods of Predicting Aircraft Rolling Moments Due to Vortex Encounters," AIAA paper 76-61.

C-8. Croom, D.R.: "Low-Speed Wind-Tunnel Investigation of Various Segments of Flight Spoilers as Trailing-Vortex-Alleviation Devices on a Transport Aircraft Model," NASA TN D-8133.

C-9. Holbrook, G.T.: "Vortex Wake Alleviation Studies with a Variable Twist Wing," NASA TP 2442.

C-10. Sammonds, R.J.: "Criteria Relating to Wake Vortex Encounter Hazard to Aircraft Response," J. Aircraft, Vol. 14, October 1977.

C-11. Johnson, W. and Rediess, H.: "Study of Control System Effectiveness in Alleviation Vortex Encounters," STI paper 141.

C-12. Hallock, J.N.: ed. "Proceeding of Aircraft Wake Vortices Conference," June 1977.

C-13. Nelson, R.C.: "Dynamic Behavior of an Aircraft Encountering Aircraft Wake Turbulence," J. Aircraft, Vol. 13, No. 9, September 1976.

1. Report No. NASA CR-187521	2. Government Accession No.	3. Recipient's Catalog No.
4. Title and Subtitle Feasibility of an Onboard Wake Vortex Avoidance System		5. Report Date April 1987 6. Performing Organization Code
7. Author(s) Alan J. Bilanin, Milton E. Teske and Howard C. Curtiss, Jr.		8. Performing Organization Report No. 87-02 10. Work Unit No.
9. Performing Organization Name and Address Continuum Dynamics, Inc. P.O. Box 3073 Princeton, New Jersey 08543		11. Contract or Grant No. NAS1-17742
12. Sponsoring Agency Name and Address National Aeronautics and Space Administration Washington, DC 20546		13. Type of Report and Period Covered Final report 14. Sponsoring Agency Code

15. Supplementary Notes

FAA/Langley D&L Field Office Technical Monitor: Harry Verstynen

16. Abstract

Landing and takeoff delays at our nation's metropolitan airports are now common place, especially during morning and early evening rush hours. These delays result primarily as a consequence of separation standards which have been established as a consequence of vortex wake concerns. The long term solution is wake alleviation but a short term solution might be an onboard vortex avoidance system. A study has been completed which has concluded that on onboard vortex wake detection system using existing, proven instrumentation is technically feasible. This system might be incorporated into existing onboard systems such as a wind shear detection system, and might provide the pilot with the location of the vortex wake, as well as an evasive manuever so that landing separations may be reduced. It is suggested that this system might be implemented into our nation's commuter aircraft fleet and major air carrier fleet and permit a reduction of current landing separation standards thereby reducing takeoff and departure delays.

17. Key Words (Suggested by Author(s))	18. Distribution Statement		
Wake vortex avoidance Onboard vortex detection	Unclassified - Unlimited Subject Category 03		
19. Security Classif. (of this report) Unclassified	20. Security Classif. (of this page) Unclassified	21. No. of Pages	22. Price*

*For sale by the National Technical Information Service, Springfield, Virginia 22161